haematologica
Journal of the Ferrata Storti Foundation

UV-induced mutations accumulate during early clonal expansion in aneuploid subtypes of pediatric B-cell precursor acute lymphoblastic leukemia

by Lianne C. Suurenbroek, Cédric G. van der Ham, Judith M. Boer, Lucca L.M. Derks, Rico Hagelaar, Markus J. van Roosmalen, Puk Klamer, Edwin Sonneveld, Monique L. den Boer, Ruben van Boxtel, Frank N. van Leeuwen, Jan L.C. Loeffen and Roland P. Kuiper

Received: October 29, 2025.
Accepted: March 30, 2026.

Citation: Lianne C. Suurenbroek, Cédric G. van der Ham, Judith M. Boer, Lucca L.M. Derks, Rico Hagelaar, Markus J. van Roosmalen, Puk Klamer, Edwin Sonneveld, Monique L. den Boer, Ruben van Boxtel, Frank N. van Leeuwen, Jan L.C. Loeffen and Roland P. Kuiper. UV-induced mutations accumulate during early clonal expansion in aneuploid subtypes of pediatric B-cell precursor acute lymphoblastic leukemia. Haematologica. 2026 Apr 9. doi: 10.3324/haematol.2025.300118 [Epub ahead of print]

UV-induced mutations accumulate during early clonal expansion in aneuploid subtypes of pediatric B-cell precursor acute lymphoblastic leukemia

Lianne C. Suurenbroek[1,*], Cédric G. van der Ham[1,*], Judith M. Boer[1], Lucca L.M. Derks[1,2], Rico Hagelaar[1,2], Markus J. van Roosmalen[1,2], Puk Klamer[1], Edwin Sonneveld[1,3], Monique L. den Boer[1], Ruben van Boxtel[1,2], Frank N. van Leeuwen[1], Jan L.C. Loeffen[1], Roland P. Kuiper[1,4]

[1] Princess Máxima Center for Pediatric Oncology, Utrecht, The Netherlands
[2] Oncode Institute, Utrecht, The Netherlands
[3] Dutch Childhood Oncology Group, Utrecht, The Netherlands
[4] Department of Genetics, Utrecht University Medical Center, Utrecht University, The Netherlands
*LCS and CGH contributed equally as co-first authors

Short title
UV damage during early clonal expansion in ALL

Corresponding author
Roland P. Kuiper. r.kuiper@prinsesmaximacentrum.nl

Data availability
The RNAseq (EGAD00001015598), whole genome sequencing (EGAD00001015599, EGAD00001015600) and single-cell whole genome sequencing data (EGAD00001015601)

Funding
This study was funded by a grant from the Dutch Cancer Society (grant no. 12482)

Disclosures
The authors declare no conflicts of interest.

Code availability
Code used in this study is publicly available on Zenodo at https://doi.org/10.5281/zenodo.18622757

Author contributions

Lianne C. Suurenbroek: Conceptualization; data curation; formal analysis; investigation; methodology; software; validation; visualization; writing - original draft preparation; writing - review & editing. **Cédric G. van der Ham**: Conceptualization; data curation; formal analysis; investigation; methodology; validation; visualization; writing - original draft preparation; writing - review & editing. **Judith M. Boer**: Resources. **Lucca L.M. Derks**: Resources. **Rico Hagelaar**: Resources; software. **Markus J. van Roosmalen**: Resources; software. **Puk Klamer**: Investigation. **Edwin Sonneveld**: Resources. **Monique L. den Boer**: Resources. **Ruben van Boxtel**: Resources. **Frank N. van Leeuwen**: Funding acquisition; writing - review & editing. **Jan L.C. Loeffen**: Resources. **Roland P. Kuiper:** Conceptualization; funding acquisition; project administration; supervision; writing - original draft preparation; writing - review & editing.

Abstract

Prolonged exposure to ultraviolet (UV) light leads to DNA damage, causing mutation accumulation and cancer, particularly in the skin. Recent studies revealed that patients with aneuploid subtypes of pediatric B-cell precursor acute lymphoblastic leukemia (BCP-ALL) commonly present with single base substitution signature 7a (SBS7a), a hallmark of UV-based DNA damage, but its origin is unclear. We screened a cohort of 191 whole genome sequenced BCP-ALL cases and confirmed the presence of SBS7a in high hyperdiploid, iAMP21 and low hypodiploid subtypes. Screening of an in-house pediatric pan-cancer cohort (n=1033) detected SBS7a, apart from BCP-ALL, only in tumors with proven cutaneous localization. Subsequent characterization of 43 BCP-ALL samples from 27 SBS7a-positive patients revealed no causative DNA repair defects. Furthermore, the mutational characteristics in SBS7a-positive BCP-ALL were very similar to those encountered in SBS7a-positive adult skin cancers (n=273) and pediatric cutaneous anaplastic large cell lymphomas (n=7), suggesting a shared UV-induced etiology. Subtle differences in aneuploid patterns were observed between SBS7a-positive and SBS7a-negative high hyperdiploid and iAMP21 cases. In several cases, we detected SBS7a-positive subclones at primary diagnosis, or relapses with apparently newly acquired SBS7a-associated mutations, together suggesting prolonged UV damage during expansion. Single-cell whole genome sequencing in two other cases confirmed some level of SBS7a-induced clonal diversity, but no indications for ongoing SBS7a-associated mutagenesis during bone marrow progression. Our data suggest that SBS7a-associated mutations occur in a subset of aneuploid BCP-ALL subtypes due to UV-induced damage during early expansion in extramedullary sites before bone marrow expansion.

Introduction

Acute lymphoblastic leukemia is the most common type of childhood cancer, with an estimated one in every 1500 newborns developing acute lymphoblastic leukemia before their 18th birthday.[1] Roughly 85% is of B-cell precursor origin. Recently, multiple studies have investigated the mutational processes which play a role during B-cell precursor acute lymphoblastic leukemia (BCP-ALL) development. Surprisingly, single base substitution signature 7a (SBS7a), which had previously been identified in skin-localized cancers and associated with damage by ultraviolet (UV) light,[2–5] was detected in specific BCP-ALL subtypes associated with aneuploidies.[6–9]

BCP-ALL has a very low mutational load,[4] but a small subset of patients is affected by mutational processes, evidenced by mutational signatures like SBS7a, that can increase the mutational load over tenfold.[8,9] Currently, the presence of SBS7a has been reported in three BCP-ALL subtypes: 15% of high hyperdiploid, 30% of near haploid and 50% of iAMP21 cases.[8–10] These subtypes share the amplification or retention of chromosome 21, while the majority of other subtypes are defined by genomic rearrangements, like gene fusions.[11] Yet, it is not understood why SBS7a in BCP-ALL only occurs in these specific subtypes.

SBS7a has been strongly associated with UV light as it is prevalent in sun-exposed skin cancers and can be induced in cell lines by exposure to UV light.[3,12] UVB light can induce the formation of pyrimidine dimers, which can lead to cytosine-to-thymine (C>T) mutations, resulting in SBS7a or, in the case of two adjacent cytosine-to-thymine mutations (CC>TT), double base substitution signature 1 (DBS1).[4,13] This DNA damage from UV light has clear characteristics, such as a bias towards untranscribed regions due to transcription-coupled nucleotide excision repair (TC-NER).[14] In addition to various skin cancers, UV light induced DNA damage has also been reported in cutaneous T-cell lymphoma, while absent in non-cutaneous T-cell lymphoma.[15]

BCP-ALL is a disease primarily occurring in the bone marrow and blood. Although UV light has been shown to cause SBS7a *in vitro*,[3] UV light cannot penetrate through the dermis and is therefore unlikely to reach the bone marrow.[16] Yet, BCP-ALL cells and healthy memory T-cells can present with SBS7a.[9,17] As such, it is still unknown if SBS7a in BCP-ALL truly results from UV light or from a different mutational process that mimics UV light-induced DNA damage. Whether there are underlying DNA repair defects or specific expression patterns underlying the subtype-specific presence of SBS7a in BCP-ALL is also unclear, though patients of European ancestry appear to be more susceptible.[9] Another open question is where, when and how long BCP-ALL cells get exposed to the mutagenic mechanism that causes SBS7a. In this study, we thoroughly characterized the mutational characteristics in SBS7a-positive BCP-ALL from 27 patients in comparison to 273 cancers with confirmed UV exposure. In addition, we performed subtype-specific comparisons in expression profiles and aneuploidy patterns between SBS7a-positive and SBS7a-negative cases and investigated the timing and clonal diversity during SBS7a acquisition.

Methods

Cohort selection

We selected SBS7a-positive pediatric BCP-ALL cases from a retrospective whole genome sequenced cohort of multiply relapsed ALL patients,[18] a retrospective whole exome sequenced cohort of relapsed ALL patients, a retrospective whole exome sequenced cohort of high hyperdiploid ALL, iAMP21 ALL and Down syndrome ALL patients and an in-house prospective whole genome sequenced effort of newly diagnosed ALL patients (Table S1). Patients selected from whole exome sequenced cohorts were subsequently whole genome sequenced for validation of SBS7a and inclusion in the study. Whole genome sequencing was performed at Novogene, Hartwig Medical Foundation or Princess Máxima Center for Pediatric Oncology using Illumina Novaseq 6000 (Illumina, 20012850) to generate 150 base-pair paired-end reads (Table S1). Samples and data were obtained from the biobank of the Dutch Childhood Oncology Group and the Princess Máxima Center. In accordance with the Declaration of Helsinki, informed written consent was obtained from all patients and/or their legal guardians before enrolment in the study and the Princess Máxima Center institutional review board approved the use of excess diagnostic material and data for this study (PMCLAB2019.054, PMCLAB2020.160 & PMCLAB2021.279).

Mutational signature analysis

Mutational matrices were generated using MutationalPatterns v3.4.1.[19] For SBSs, de novo signature extraction was performed using NMF v0.26[20] with a rank of 6 (BCP-ALL) or 8 (pan-cancer). MutationalPatterns v3.4.1 was used to refit the extracted signatures with COSMIC signatures, and the 7 (BCP-ALL) or 11 (pan-cancer) resulting signatures were used to perform a refit of the mutational matrix (Table S2 & S3). For samples with a positive contribution for SBS7a, a bootstrap with 100 iterations was performed with MutationalPatterns v3.4.1.[19] Samples were marked as SBS7a-positive if they i) showed a positive contribution of SBS7a, ii) could be reconstructed with a cosine similarity of at least 0.9, and iii) had a positive SBS7a contribution in at least 90% of bootstraps.

Single-cell WGS

Cells were stained using APC-CD10 (biolegend, 312209) and DAPI to select living CD10+ lymphoblasts, and sorted for sequencing according to Derks et al[21]. Primary template-directed DNA amplification was performed using the ResolveDNA® Whole Genome Amplification Kit – 96 Reactions (BioSkryb 100136).[21] Mesenchymal stromal cells (MSCs) were cultured in bulk, and DNA from these cells was extracted with the QIAamp DNA Micro Kit and used as germline control. Libraries were prepared using TruSeq Nano kit (Illumina, 20015965), and sequenced with the Novaseq 6000 (Illumina, 20012850) for 2 x 150 bp paired-end reads.

Additional method description is given in the supplementary data.

Results

BCP-ALL cases with SBS7a

To study SBS7a in BCP-ALL we collected SBS7a-positive BCP-ALL samples from 27 patients treated at the Princess Máxima Center for Pediatric Oncology (Figure 1A). Seventeen of these were identified by mutational signature analysis on an unselected cohort of 191 BCP-ALL samples diagnosed between 2019 and 2023, revealing a prevalence of 9% and a relative contribution of SBS7a to the mutational spectrum from 10 to 100% (median 36%). In line with previous studies,[8–10] SBS7a was enriched in three specific subtypes, specifically 50% of the iAMP21 cases (4 out of 8), 20% of the low hypodiploid cases (1 out of 5) and 16% of the high hyperdiploid cases (12 out of 74) presented with SBS7a (Figure 1B). These subtypes typically present with copy number alterations of chromosome 21. The remaining ten samples were from multiple retrospective BCP-ALL cohorts (Table S1).[18,22] In total, we included 16 high hyperdiploid, nine iAMP21, one low hypodiploid and one B-other case (Figure 1A). SBS7a was usually detected at initial diagnosis, but in two cases the first appearance of SBS7a was in a relapse sample. We did not find significant differences in age at initial diagnosis between SBS7a-negative and SBS7a-positive cases for any of the BPC-ALL subtypes (P=0.35), indicating that the increased tumor mutational load is not aging related (Figure 1C).

SBS7a in other pediatric cancers

Next, we investigated the prevalence of SBS7a-associated mutations in other pediatric cancers than BCP-ALL. To this end, we analyzed a pediatric pan-cancer cohort of 1033 whole genome sequenced tumors from the Princess Máxima Center for Pediatric Oncology (Table 1). Except for one melanoma, all SBS7a-positive malignancies were of hematological origin (Table 1) which, apart from BCP-ALL, included one B-cell lymphoblastic lymphoma (iAMP21 subtype) and seven anaplastic large cell lymphomas (ALCL) (Table 1). The melanoma and B-cell lymphoblastic lymphoma had a cutaneous localization. The ALCL cases often presented with multiple lesions, of which some were cutaneous (Table S4). One BCP-ALL relapse, which presented with SBS7a, was found to be located in the patient's eye. Therefore, whereas in the majority of SBS7a-positive BCP-ALLs an association with UV exposure is unclear, other pediatric cancers with SBS7a-associated DNA damage were exclusively found in sun-exposed lesions.

Characteristics of UV damage in BCP-ALL subtypes

UV exposure introduces pyrimidine dimers that can result in cytosine-to-thymine mutations, which, apart from the single base substitution signature SBS7a, includes an enrichment of CC>TT double base substitutions (signature DBS1). Furthermore, as observed in sun-exposed tissues, SBS7a and DBS1 present with transcriptional strand asymmetry.[4,14] We therefore performed a comprehensive comparison of mutational characteristics in SBS7a-positive BCP-ALLs with those in skin cancer, where UV as the source of SBS7a is well established (Supplementary methods).[12] We used a previously characterized cohort of adult metastatic skin cancer,[23] and included the seven pediatric ALCL cases from our cohort in this analysis. Although SBS7a-positive skin cancers showed a 27.4-fold higher mutational load than SBS7a-positive BCP-ALL (P=2.2×10^{-15}), mutational load in these BCP-ALLs was still 2.6-fold higher than SBS7a-negative BCP-ALL and like SBS7a-positive ALCL (Figure 2A, P=2.1×10^{-8}). Similarly, the load of DBS1 (CC>TT mutations) was significantly higher in skin cancer (P=2.7×10^{-15}), but the ratio of CC>TT compared to single C>T mutations was similar in all SBS7a-positive tumors (Figure 2B). Additionally, the well-established bias for the untranscribed strand in skin cancer, caused by TC-NER[14], was also present in SBS7a-positive BCP-ALL and ALCL, but

not in SBS7a-negative BCP-ALL (Figure 2C, $P=2.4\times10^{-6}$). The stronger transcriptional strand bias in the skin cancer samples ($P=2.6\times10^{-6}$) likely resulted from the far greater proportion of SBS7a-associated mutations relative to mutations associated with other mutational signatures in the C>T spectrum without transcriptional strand bias, like SBS1. Overall, the characteristics of SBS7a in BCP-ALL are indistinguishable from SBS7a in cancers with established UV-induced mutations, with the only notable difference being the number of SBS7a-associated mutations. These findings confirm that mutagenesis in SBS7a-positive BCP-ALL takes place through the formation of pyrimidine dimers, the established direct consequence of UV damage. This is in line with a previous study that reported that SBS7a is more common in BCP-ALL patients of European ancestry compared to those of African ancestry.[9]

No recurrent nucleotide excision repair pathway mutations in SBS7a-positive BCP-ALL

The main DNA repair pathway for UV light-induced DNA damage is nucleotide excision repair (NER), and defects in this pathway can exacerbate the acquisition of mutations after UV light exposure.[13,24,25] Therefore, we investigated if SBS7a-positive BCP-ALL samples harbored NER pathway mutations that could lead to a higher sensitivity to UV-associated DNA damage. To this end, we investigated all genes attributed to the NER pathway in the Kyoto Encyclopedia of Genes and Genomes (Table S5, Supplementary methods), using our genomic and transcriptomic data.[26] We did not detect any pathogenic NER pathway mutations or aberrant expression of NER pathway genes in SBS7a-positive BCP-ALL (Figure S1, Table S6). This is in line with the presence of transcriptional strand bias, which indicates active TC-NER. Therefore, NER pathway defects are not responsible for the acquisition of SBS7a in BCP-ALL.

The presence of SBS7a is not associated with transcriptional changes

We then investigated if the presence of SBS7a could be explained by, or result in, expression of other specific genes or pathways. Therefore, we performed differential expression analysis of SBS7a-positive and SBS7a-negative samples in the high hyperdiploid and iAMP21 subgroups separately. For validation, we used a cohort of 118 high hyperdiploid and 27 iAMP21 cases from the St. Jude Children's Research Hospital,[27] in which the SBS7a mutation contribution was determined (Methods). Whereas differentially expressed genes were identified in each of the datasets, none of these genes were recurrently found in all datasets (Figure S2). Two upregulated genes overlapped between the iAMP21 cohorts, but these genes were not differentially expressed in the high hyperdiploid samples.
When comparing iAMP21 and high hyperdiploid BCP-ALL to *ETV6*::*RUNX1* BCP-ALL, we found no overlapping gene sets which could explain the presence of SBS7a (Figure S3). However, when genes commonly upregulated across aneuploid subtypes were selected, an enrichment of several GO terms involved in migration was found (Figure S4, Table S7). Although speculative, this enrichment may underlie a stronger potential of aneuploid BCP-ALL subtypes to migrate to extramedullary sites, providing an explanation for the subtype-specific presentation of SBS7a.

Aneuploidy patterns in SBS7a-positive ALL

The restricted presence of SBS7a in aneuploid BCP-ALL subtypes suggests that specific copy number aberrations may be involved in a temporal skin localization or in higher susceptibility to UV light. Therefore, we investigated these aneuploidy patterns in more

detail. We were able to confirm earlier studies demonstrating that SBS7a-associated mutations in high hyperdiploid and iAMP21 BCP-ALL were generally not duplicated on amplified chromosomes, and thus occurred after the subtype-defining ploidy alterations (Figure S5, Supplementary methods).[9,10]

The high hyperdiploid subtype can present with different combinations of amplified chromosomes. Besides the obligatory amplification of chromosome 21, chromosomes 4, 6, 10, 14, 17, 18 and X are often amplified, while amplification of other chromosomes is much less common.[28] For a comparison of the aneuploidy patterns between SBS7a-positive and SBS7a-negative high hyperdiploid BCP-ALL samples, we expanded our dataset with a cohort of high hyperdiploid patients from the St. Jude Children's Research Hospital[27] to a cohort of 219 cases of which 40 were SBS7a-positive (Figure 3A). Clustering analysis did not reveal a globally different pattern between the two groups, but chromosome-specific analyses showed that amplification of chromosome 4 and 17 was slightly less common in SBS7a-positive patients in both cohorts (Figure 3A, Table S8, Supplementary methods). This difference was not due to a general difference in the number of whole chromosome gains (Table S9). Since chromosomal amplification patterns in high hyperdiploid BCP-ALL involving chromosomes 5, 17, 18, and 20 were previously shown to impact prognosis,[29] we tested whether an association could be found between these risk groups and the presence of SBS7a, but such an association was not found (Figure 3B, *P*=0.60). We also analyzed other known recurrent alterations in high hyperdiploid BCP-ALL, specifically 1q gain, 6q deletion, isochromosome 7q and isochromosome 17q,[28] and found no association with SBS7a (Table S8). As the copy number of chromosome 21 in high hyperdiploid BCP-ALL can vary between three and five copies,[30] we analyzed the amount of additional copies of chromosome 21 in SBS7a-positive and SBS7a-negative patients and found no significant difference (Figure 3C, *P*=0.31). Finally, we compared the chromosome 21 amplification patterns between SBS7a-negative and SBS7a-positive iAMP21 cases, again using an extended cohort,[27] which revealed two regions that seemed to differ in average copy number between SBS7a-negative and SBS7a-positive patients (Figure 3D). The second region, at the end of the q-arm, was more amplified in SBS7a-negative cases (*P*=0.01), although this did not result in differential expression of genes (Figure S2). Altogether, SBS7a in high hyperdiploid and iAMP21 BCP-ALL appears to be associated with very subtle differences in commonly amplified regions.

SBS7a-associated mutations in minor subclones

Whereas the likelihood that a (pre)leukemic cell is exposed to UV appears to be subtype dependent, the mutagenic consequences may also depend on the duration of UV exposure. Furthermore, expansion of a preleukemic clone during UV exposure may even result in clonal heterogeneity and relapse. To obtain more insight into this process, we investigated whether these mutations accumulate during clonal evolution of BCP-ALL, resulting in subclones with newly acquired SBS7a mutations, or whether they would be found only in the major clone. We selected six patients from our cohort that showed a bimodal split in allele frequency (AF) distribution, indicating the presence of a major clone and one or more subclones, each harboring at least 200 mutations (Figure S6). In three patients, SBS7a contribution was high in the major clone, but the minor clone(s) carried no additional SBS7a mutations (Figures 4A and S7). In contrast, the other three cases showed high levels of subclonal SBS7a-associated mutations, suggesting a prolonged UV exposure (Figures 4B and

S7). These findings suggest that UV-associated mutagenesis is not restricted to a single leukemia-initiating cell but contributes to clonal heterogeneity in at least a subset of cases.

New appearance of UV-induced mutations in BCP-ALL relapses

In line with the above observation, we noticed that seven out of ten relapsed BCP-ALL cases presented with additional SBS7a-associated mutations at time of relapse (Figure 1A). To determine whether these mutations could be traced back at initial diagnosis, we selected three cases for in-depth analysis. Each case presented with SBS7a at initial diagnosis and acquired new SBS7a mutations at first relapse (Figure 5, Supplementary methods). We then selected relapse-specific mutations with high likelihood of being caused by SBS7a, and performed amplicon-based deep sequencing on the initial diagnosis (median depth ~20,000) and first relapse (median depth ~6,000) samples of the three cases. In all three cases, mutations were only detected in the relapse samples. At initial diagnosis, the AF of all mutations was indistinguishable from the negative control samples (Figure 5, P=0.84, P=0.42, P=0.63). These results show that SBS7a mutations found in relapse samples either originated from a subclone at initial diagnosis that was undetectable in the sample due to clone size or location in the bone marrow, or were truly newly acquired.

Relapse-specific mutations can arise because they are positively selected for, for example by conferring drug resistance.[6,7] We found that two mutations in *NR3C1* and three mutations in *CREBBP* have a high probability of being caused by SBS7a (Figure S8). Since both genes are implicated in glucocorticoid resistance, SBS7a might have played a role in disease progression.[7]

SBS7a stops accumulating in the final stage of disease progression

Considering the observation that UV-associated damage proceeds in a prolonged period of time, we finally addressed the question whether SBS7a-associated mutations encountered in BCP-ALL represent a past mutational event or a process that is still ongoing during expansion in the bone marrow. Therefore, we performed single-cell WGS on the initial diagnosis samples of two patients with high hyperdiploid BCP-ALL (P0624 and P0625). For each of these samples, thirteen single cells were sorted, and primary template-directed amplification followed by whole genome sequencing was performed. The single-cell data corresponded well with the bulk WGS data, as for each of these samples, 92% and 91% of the mutations identified in the bulk WGS data were also identified in the single-cell WGS data. We then built a lineage tree to infer clonal evolution and identify subclonal populations. Both lineage trees showed a trunk that contained the mutations we previously detected in the bulk WGS data. For both patients the trunk of the tree, containing mutations identified in all cells, showed a large contribution of SBS7a. In P0625 (Figure 6), two cells individually branch off during early leukemic development. We attribute these branches to lower data quality for these two cells (Figure S9), which suggest that branches X, F, and G actually all belong to the main trunk. However, branch P, which contained mutations shared by four cells, was of good quality. The mutations shared in this branch had a reduced AF in the tumor bulk (P<2.2×10^{-16}), which indicates that the four cells originating from branch P are part of an SBS7a-positive subclone (Figure 6). In contrast, none of the unique mutations in each of these cells (mean 219, range 175-284) showed SBS7a contribution. In P0624 (Figure S10), we identified two subclonal branches with sufficient quality, branch U and

branch W, that do not contain SBS7a (Figures S9 and S10). Furthermore, similar to P0625, the private branches for all cells in patient P0624 contain only unique mutations (mean 260, range 190-298) which are not associated with SBS7a (Figure S10). Since these mutations represent the latest stages of leukemic development, these data suggest that SBS7a is not acquired during progression in the bone marrow.

Discussion

The presence of SBS7a, a well characterized mutational signature linked to UV light-induced DNA damage, was recently reported in aneuploid subtypes of BCP-ALL[31] and then confirmed by several studies.[6,8,9] In this study we identified UV light as the most likely source for SBS7a mutations in BCP-ALL. Additionally, we provide indications that SBS7a-positive BCP-ALL subtypes are exposed to UV light for a prolonged period during early clonal expansion, resulting in subclonal diversity. These results suggest that preleukemic B lymphoblasts with aneuploid karyotypes tend to migrate to and reside in sun-exposed tissues, where they may accumulate UV-induced mutations while undergoing clonal expansion.

A role for UV light in mutation accumulation in BCP-ALL is unexpected in a disease that predominantly develops in the bone marrow. Apart from BCP-ALL, SBS7a has been found in skin cancer, T-cell lymphomas and, as we show in this study, pediatric ALCL,[4,12,15] where UV exposure as a source of these mutations is plausible. Furthermore, we identified one case in which SBS7a-associated mutations appeared only at relapse in the eye. Consistent with established UV-induced malignancies,[24,32] BCP-ALL presents with pyrimidine dimer formation, followed by mutation incorporation through translesion synthesis.[24,32] So far, the formation of pyrimidine dimers has only been described as a consequence of UV exposure,[24] with no other known inducers of pyrimidine dimers.[3] Although there are chemicals that can induce the formation of DNA adducts, such as psoralen and alkylating agents, these are known to induce different mutational signatures.[3,33] As for endogenous processes, reactive oxygen species can also cause DNA adducts, but result in another mutational signature.[2] These findings are all in line with the previously observed trend that SBS7a occurs more frequently in BCP-ALL patients of European ancestry than patients of African ancestry, further suggesting that there is an association with sensitivity to UV light.[33–37] Therefore, UV exposure remains the most likely explanation for SBS7a in BCP-ALL.

The most likely scenario by which BCP-ALL can be exposed to UV light is localization in the skin prior to or during (early stages of) leukemia development. Skin lesions in BCP-ALL are rare,[34–38] but may remain small or temporary, and thus underreported. Hematopoietic stem and progenitor cells (HSPCs) can circulate in the peripheral blood, home to sites of injury, including the skin, and return to the bone marrow.[39–41] Additionally, a release of large numbers of HSPCs from the bone marrow can also be triggered by numerous stress conditions.[40] Perhaps, B lymphoblasts can also migrate to extramedullary sun-exposed tissues under certain conditions.

Migration of B lymphoblasts to the skin could be triggered by early driver events. SBS7a in BCP-ALL shows a striking subtype specificity, being mostly restrained to aneuploid BCP-ALL subtypes with amplification or retention of chromosome 21,[9,10] and these amplifications

always precede the accumulation of SBS7a. However, not all such cases show SBS7a, suggesting that aneuploidies might infer a risk instead of directly causing SBS7a mutation accumulation. We found minor differences in copy number profiles, which could affect the expression of specific genes that influence the likelihood for temporal localization and/or expansion in sun-exposed areas, resulting in higher chance of SBS7a-accumulation. Since we found no overall differences in gene expression profiles between SBS7a-positive and -negative BCP-ALL cases, these cases do not appear to be intrinsically different leukemias and thus may in general behave similarly. Additionally, we found some indications that subtype-specific expression might increase the capability of cell migration. This suggests that SBS7a accumulation is a stochastic process, but has higher likelihood to occur in the presence of certain primary subtype-specific aberrations.

The increased tumor mutational load in SBS7a-positive BCP-ALL compared to SBS7a-negative cases and the detection of relapse-specific SBS7a mutations indicate prolonged exposure to UV light. Additionally, using both bulk and single-cell WGS, we found that SBS7a mutations can be present in subclones. In later stages of development, however, no new SBS7a mutations seem to be acquired. These results indicate that SBS7a mutations accumulate over time during initial stages of clonal expansion, before further progression in the bone marrow.

Altogether, we propose a model in which (pre)malignant aneuploid BCP-ALL cells temporarily end up in the skin, where they get exposed to UV light while they expand as a (premalignant) lesion. The total amount of UV exposure, and the subsequent mutational consequences, may vary from case to case. Preleukemic cells from such a lesion may return to the blood stream and home to the bone marrow where they potentially progress to overt leukemia. Continued release of cells from such a lesion, which may home at different sites in the bone marrow, could explain the clonal heterogeneity we detected in BCP-ALL. Such a model would also be consistent with our observation that some relapses present with SBS7a mutations that were not detected in the sample taken at initial diagnosis, although re-exposures after initial diagnosis cannot be excluded. So far, research into the motility of ALL cells has mainly focused on the differences between B- and T-lineage ALL,[42,43] and it would be interesting to see future studies explore the motility differences between the various BCP-ALL subtypes. Based on our model, we expect that aneuploid subtypes of BCP-ALL show increased motility, leading to the possibility of SBS7a mutation acquisition in sun-exposed tissues.

A key limitation of our study is that it does not resolve why SBS7a arises almost exclusively in aneuploid BCP-ALL subtypes. Whether this reflects increased vulnerability of these cells to UV-induced mutagenesis, or a biological tendency to reside or persist in environments where UV exposure is possible, remains unknown. Addressing this would require experimentally demanding approaches, including subtype-specific UV exposure models, migration or skin-homing assays, and *in vivo* systems that capture transient or pre-diagnostic extramedullary phases. Such models are currently limited or not physiologically representative. Consequently, while our data support UV exposure during early clonal evolution, the upstream cause of subtype specificity remains unresolved.

In conclusion, we show that temporal exposure to UV light is the most likely cause of SBS7a in BCP-ALL. It remains unknown if SBS7a mutations can alter the development of BCP-ALL. We have found that SBS7a acquisition can introduce pathogenic driver mutations,[18] so SBS7a acquisition might play a role in the onset of BCP-ALL, or even induce therapy resistance in individual cases. However, this remains very speculative, and further studies on large cohorts will need to prove if SBS7a mutations can influence the prognosis of patients with BCP-ALL. Although the clinical relevance of SBS7a in BCP-ALL remains unknown, the mechanisms of SBS7a mutation accumulation give insight into the origins and development of BCP-ALL.

References

1. Pieters R, Mullighan CG, Hunger SP. Advancing diagnostics and therapy to reach universal cure in childhood ALL. J Clin Oncol. 2023;41(36):5579-5591.
2. Alexandrov LB, Nik-Zainal S, Wedge DC, et al. Signatures of mutational processes in human cancer. Nature. 2013;500(7463):415-421.
3. Kucab JE, Zou X, Morganella S, et al. A compendium of mutational signatures of environmental agents. Cell. 2019;177(4):821-836.e16.
4. Alexandrov LB, Kim J, Haradhvala NJ, et al. The repertoire of mutational signatures in human cancer. Nature. 2020;578(7793):94-101.
5. Mata DA, Williams EA, Sokol E, et al. Prevalence of UV mutational signatures among cutaneous primary tumors. JAMA Netw Open. 2022;5(3):e223833.
6. Li B, Brady SW, Ma X, et al. Therapy-induced mutations drive the genomic landscape of relapsed acute lymphoblastic leukemia. Blood. 2020;135(1):41-55.
7. Waanders E, Gu Z, Dobson SM, et al. Mutational landscape and patterns of clonal evolution in relapsed pediatric acute lymphoblastic leukemia. Blood Cancer Discov. 2020;1(1):96-111.
8. Studd JB, Cornish AJ, Hoang PH, Law P, Kinnersley B, Houlston R. Cancer drivers and clonal dynamics in acute lymphoblastic leukaemia subtypes. Blood Cancer J. 2021;11(11):177.
9. Brady SW, Roberts KG, Gu Z, et al. The genomic landscape of pediatric acute lymphoblastic leukemia. Nat Genet. 2022;54(9):1376-1389.
10. Gao Q, Ryan SL, Iacobucci I, et al. The genomic landscape of acute lymphoblastic leukemia with intrachromosomal amplification of chromosome 21. Blood. 2023;142(8):711-723.
11. Iacobucci I, Kimura S, Mullighan CG. Biologic and therapeutic implications of genomic alterations in acute lymphoblastic leukemia. J Clin Med Res. 2021;10(17):3792.
12. Hayward NK, Wilmott JS, Waddell N, et al. Whole-genome landscapes of major melanoma subtypes. Nature. 2017;545(7653):175-180.
13. Mullenders LHF. Solar UV damage to cellular DNA: from mechanisms to biological effects. Photochem Photobiol Sci. 2018;17(12):1842-1852.
14. Otlu B, Díaz-Gay M, Vermes I, et al. Topography of mutational signatures in human cancer. Cell Rep. 2023;42(8):112930.
15. Jones CL, Degasperi A, Grandi V, et al. Spectrum of mutational signatures in T-cell lymphoma reveals a key role for UV radiation in cutaneous T-cell lymphoma. Sci Rep. 2021;11(1):3962.
16. D'Orazio J, Jarrett S, Amaro-Ortiz A, Scott T. UV radiation and the skin. Int J Mol Sci. 2013;14(6):12222-12248.
17. Machado HE, Mitchell E, Øbro NF, et al. Diverse mutational landscapes in human lymphocytes. Nature. 2022;608(7924):724-732.
18. van der Ham CG, Suurenbroek LC, Kleisman MM, et al. Mutational mechanisms in multiply relapsed pediatric acute lymphoblastic leukemia. Leukemia. 2024;38(11):2366-2375.
19. Manders F, Brandsma AM, de Kanter J, et al. MutationalPatterns: the one stop shop for the analysis of mutational processes. BMC Genomics. 2022;23(1):134.
20. Gaujoux R, Seoighe C. A flexible R package for nonnegative matrix factorization. BMC Bioinformatics. 2010;11:367.

21. Derks LLM, van Leeuwen AJCN, Steemers AS, et al. Protocol for genome-wide analysis of somatic variants at single-cell resolution using primary template-directed DNA amplification. STAR Protoc. 2025;6(1):103499.
22. Hormann FM, Østergaard A, van den Broek S, et al. Secondary lesions and sensitivity to signaling inhibitors in iAMP21 acute lymphoblastic leukemia. Hemasphere. 2025;9(1):e70069.
23. Priestley P, Baber J, Lolkema MP, et al. Pan-cancer whole-genome analyses of metastatic solid tumours. Nature. 2019;575(7781):210-216.
24. Ikehata H, Ono T. The mechanisms of UV mutagenesis. J Radiat Res. 2011;52(2):115-125.
25. Lehmann AR, McGibbon D, Stefanini M. Xeroderma pigmentosum. Orphanet J Rare Dis. 2011;6:70.
26. Kanehisa M, Goto S. KEGG: kyoto encyclopedia of genes and genomes. Nucleic Acids Res. 2000;28(1):27-30.
27. McLeod C, Gout AM, Zhou X, et al. St. Jude Cloud: a pediatric cancer genomic data-sharing ecosystem. Cancer Discov. 2021;11(5):1082-1099.
28. Haas OA, Borkhardt A. Hyperdiploidy: the longest known, most prevalent, and most enigmatic form of acute lymphoblastic leukemia in children. Leukemia. 2022;36(12):2769-2783.
29. Enshaei A, Vora A, Harrison CJ, Moppett J, Moorman AV. Defining low-risk high hyperdiploidy in patients with paediatric acute lymphoblastic leukaemia: a retrospective analysis of data from the UKALL97/99 and UKALL2003 clinical trials. Lancet Haematol. 2021;8(11):e828-e839.
30. Abbasi MR, Nebral K, Haslinger S, et al. Copy number changes and allele distribution patterns of chromosome 21 in B cell precursor acute lymphoblastic leukemia. Cancers (Basel). 2021;13(18):4597.
31. Ma X, Liu Y, Liu Y, et al. Pan-cancer genome and transcriptome analyses of 1,699 paediatric leukaemias and solid tumours. Nature. 2018;555(7696):371-376.
32. Nieto Moreno N, Olthof AM, Svejstrup JQ. Transcription-coupled nucleotide excision repair and the transcriptional response to UV-induced DNA damage. Annu Rev Biochem. 2023;92(1):81-113.
33. Olafsson S, Rodriguez E, Lawson ARJ, et al. Effects of psoriasis and psoralen exposure on the somatic mutation landscape of the skin. Nat Genet. 2023;55(11):1892-1900.
34. Cho-Vega JH, Medeiros LJ, Prieto VG, Vega F. Leukemia cutis. Am J Clin Pathol. 2008;129(1):130-142.
35. Andriescu EC, Coughlin CC, Cheng CE, et al. Pediatric leukemia cutis: a case series. Pediatr Dermatol. 2019;36(5):658-663.
36. Afzal A, Mingola P, Farooque U, Shabih S, Thomas CA. B-cell acute lymphoblastic leukemia presenting as leukemia cutis: A case report. Cureus. 2020;12(10):e11032.
37. Yin Y-T, Tseng J-H, Liu Y-L, Miser JS, Chen S-H. Neonatal acute lymphoblastic leukemia (MLL-AF9) with leukemia cutis. Pediatr Neonatol. 2021;62(6):676-678.
38. Kanoje PK, Khullar G, Yadav AK, Saxena AK, Gupta DK. Generalized leukemia cutis as the initial manifestation of precursor B-cell acute lymphoblastic leukemia in a young male. Dermatol Ther. 2021;34(1):e14594.
39. Khalil S, Ariel Gru A, Saavedra AP. Cutaneous extramedullary haematopoiesis: Implications in human disease and treatment. Exp Dermatol. 2019;28(11):1201-1209.
40. Yang X, Chen D, Long H, Zhu B. The mechanisms of pathological extramedullary

hematopoiesis in diseases. Cell Mol Life Sci. 2020;77(14):2723-2738.
41. Kavanagh DPJ, Kalia N. Hematopoietic stem cell homing to injured tissues. Stem Cell Rev. 2011;7(3):672-682.
42. Barz MJ, Behrmann L, Capron D, et al. B- and T-cell acute lymphoblastic leukemias evade chemotherapy at distinct sites in the bone marrow. Haematologica. 2023;108(5):1244-1258.
43. Kanari M, Jimenez Garcia I, Steffen FD, et al. A three-dimensional ex vivo model recapitulates in vivo features and drug resistance phenotypes in childhood acute lymphoblastic leukemia. Leukemia. 2025;39(12):2881-2894.

Tables

Table 1: Prevalence of SBS7a-associated mutations in a pediatric pan-cancer cohort (n=1033)

Tumor type	Number of samples	Number of SBS7a-positive samples
Hematological Malignancies	**389**	**24 (6.2%)**
Anaplastic large cell lymphoma	9	7 (77.8%)
B-cell lymphoblastic lymphoma	3	1 (33.3%)
B-cell progenitor acute lymphoblastic leukemia	207	16 (7.7%)
Acute myeloid leukemia	60	0
T-cell acute lymphoblastic leukemia	35	0
Burkitt lymphoma	22	0
T-cell lymphoblastic lymphoma	21	0
Diffuse large B-cell lymphoma	11	0
Hodgkin lymphoma	8	0
Chronic myeloid leukemia	7	0
Primary mediastinal large B-cell lymphoma	4	0
Intestinal T-cell lymphoma	1	0
Mature T-cell lymphoma	1	0
Solid Tumors	**428**	**1 (0.2%)**
Melanoma	4	1 (25%)
Neuroblastoma	81	0
Nephroblastoma	71	0
Rhabdomyosarcoma	54	0
Osteosarcoma	48	0
Ewing sarcoma	43	0
Sarcoma other	36	0
Gonadal germ cell	18	0
Hepatoblastoma	16	0
Fibrosarcoma	13	0
Carcinoma other	8	0
Gonadal carcinoma	6	0
Gonadal other	6	0
Histiocytic neoplasm	5	0
Adrenocortical carcinoma	4	0
Nasopharyngeal carcinoma	4	0
Thyroid carcinoma	4	0
Germ cell other	3	0
Hepatic carcinoma	3	0
Renal carcinoma	1	0
Neurological Tumors	**216**	**0**
Astrocytoma	63	0
Medulloblastoma	39	0
Glioma high-grade	29	0
Ependymoma	26	0
Glioma	16	0
Atypical teratoid rhabdoid tumor	12	0
Brain high-grade	10	0
Astrocytoma high-grade	9	0
Brain other	9	0
Germ cell brain	3	0

Figure legends

Figure 1: Mutational signature SBS7a can be detected in multiple subtypes of BCP-ALL. A) Barplot depicting the total cohort of BCP-ALL patients with SBS7a-associated mutations. A colored bar was added to the x-axis that displays the subtype of each sample. If a patient relapsed, multiple bars are shown to indicate each diagnosis in chronological order. B) Percentage barplot presenting the prevalence of SBS7a in BCP-ALL. The x-axis shows the included BCP-ALL subtypes, with *DUX4* rearranged, *MEF2D* rearranged, *MYC* rearranged and near haploid (all n=1) collected in a "Other subtype" group for visual clarity. C) Boxplot comparing age at diagnosis for patients with and without SBS7a-associated mutations. Boxplots are colored to indicate the presence (yellow) or absence of (grey) of SBS7a-associated mutations. Statistical analysis was performed with two-way ANOVA.

Figure 2: Comparison of SBS7a in pediatric BCP-ALL, pediatric ALCL and adult skin cancer. A) Boxplot depicting the median mutational load in each tumor type, with the BCP-ALL samples split in SBS7a-positive and SBS7a-negative samples. B) Scatterplot showing the ratio between CC>TT mutations (y-axis) and C>T mutations (x-axis) for each tumor type, with the BCP-ALL samples split in SBS7a-positive and SBS7a-negative samples. C) Boxplot of the transcriptional strand bias of C>T mutations in each tumor type, with the BCP-ALL samples split in SBS7a-positive and SBS7a-negative samples. On the y-axis, positive values indicate a bias for the transcribed strand and negative values indicate a bias for the untranscribed strand. A-C) Color corresponds to tumor type. SBS7a-negative BCP-ALL is depicted in grey, SBS7a-positive BCP-ALL is depicted in dark orange, SBS7a-positive ALCL is depicted in orange and SBS7a-positive skin cancer is depicted in yellow. Statistical analysis was performed with the Wilcoxon rank sum test. N.S: not significant, *: $p < 0.05$, **: $p < 0.01$, ***: $p < 0.001$.

Figure 3: Copy number alterations in SBS7a-positive patients. A) Plot that depicts the amplified chromosomes in each high hyperdiploid BCP-ALL patient. Chromosomes are shown on the x-axis and colored red if amplified. Patients are clustered on the y-axis depending on their set of amplified chromosomes. The y-axis also shows if patients are SBS7a-positive (yellow) or SB7a-negative (grey), and if the patient belongs to the Princess Máxima Center cohort (orange) or St. Jude Children's Research Hospital cohort (blue). Additionally, above the plot the percentage of patients with an amplification of each chromosome is shown, for SBS7a-positive (yellow) and SBS7a-negative (grey) patients. B) Percentage bar plot showing the percentage of SBS7a-positive and SBS7a-negative high hyperdiploid BCP-ALL patients that had a good or poor prognosis according to the criteria established by Enshaei *et al*, 2021.[29] C) Percentage bar plot that indicates the number of chromosome 21 copies detected in SBS7a-positive and SBS7a-negative patients. D) Graphical representation of chromosome 21 with a line graph of the mean amplified region of chromosome 21 in iAMP21 patients. Patients were separated by cohort and presence of SBS7a. Two regions with higher variability between the four groups are highlighted and accompanied with a boxplot showing the average copy number in that region for SBS7a-negative and SBS7a-positive patients. Statistical analysis was performed with the Fisher's exact test (A, B), chi-square test (C) or Wilcoxon rank sum test (D). N.S: not significant, *: $p < 0.05$, **: $p < 0.01$, ***: $p < 0.001$.

Figure 4: Subclonal SBS7a mutations. A) In three patients, subclonal mutations that were distinct from the major clone could be identified but were not associated with SBS7a. B) Three patients had subclonal mutations which were distinct from the major clone and were associated with SBS7a. A,B) The first column depicts a violin plot of the AF of SBSs. Lines were added to indicate the split between mutations belonging to the major clone and subclonal mutations. The second column shows the mutational profile of the clonal and subclonal mutations as identified in the first column. The third column shows the absolute contribution of SBS7a-associated mutations to the clonal and subclonal mutations identified in the first column. The fourth column shows the relative number of SBS7a-associated mutations in the clonal and subclonal fraction for all patients belonging to that category. Dx: initial diagnosis, R: relapse.

Figure 5: SBS7a-associated mutations found in relapse samples cannot be detected at initial diagnosis. Each row presents data of one patient. The first column shows the number of mutations acquired at each subsequent diagnosis. The yellow coloring represents the number of mutations that were attributed to SBS7a. The second column shows the results of deep sequencing of selected mutations that were very likely introduced by SBS7a and unique to the relapse sample. The x-axis and the coloring of the dots show if the mutation was sequenced in control samples (orange), the initial diagnosis sample (blue) or the relapse sample (green). Each dot represents a unique mutation. The third column depicts fish plots that represent the evolution of each tumor. Each clone is given a different color and the percentage of SBS7a-associated mutations in each clone is shown in the legend. Statistical analysis was performed with the Wilcoxon rank sum test. N.S: not significant, *: $p < 0.05$, **: $p < 0.01$, ***: $p < 0.001$.

Figure 6: Lineage tree based on the single-cell WGS data of patient P0625. A) Lineage tree. The trunk of the lineage tree shows the number of shared mutations between all following clones. If a clone branches off, it means that it shares no more mutations with other clones. The number of mutations is depicted above each branch along with a pie chart that shows the percentage of mutations associated with each mutational signature. SBS7a is shown in yellow, SBS1 is shown in blue and other mutational signatures are shown in white. To the right of the lineage tree is a bar plot corresponding to each clone in the lineage tree. This bar plot shows whether over 75% of the genome is covered with a depth of at least 5 (green bars). B) Mutational profiles of each group of shared mutations that had a contribution of SBS7a. C) Boxplot that shows the allele AF for each group of shared mutations that contained SBS7a-associated mutations. Statistical analysis was performed with the Wilcoxon rank sum test. N.S: not significant, *: $p < 0.05$, **: $p < 0.01$, ***: $p < 0.001$.

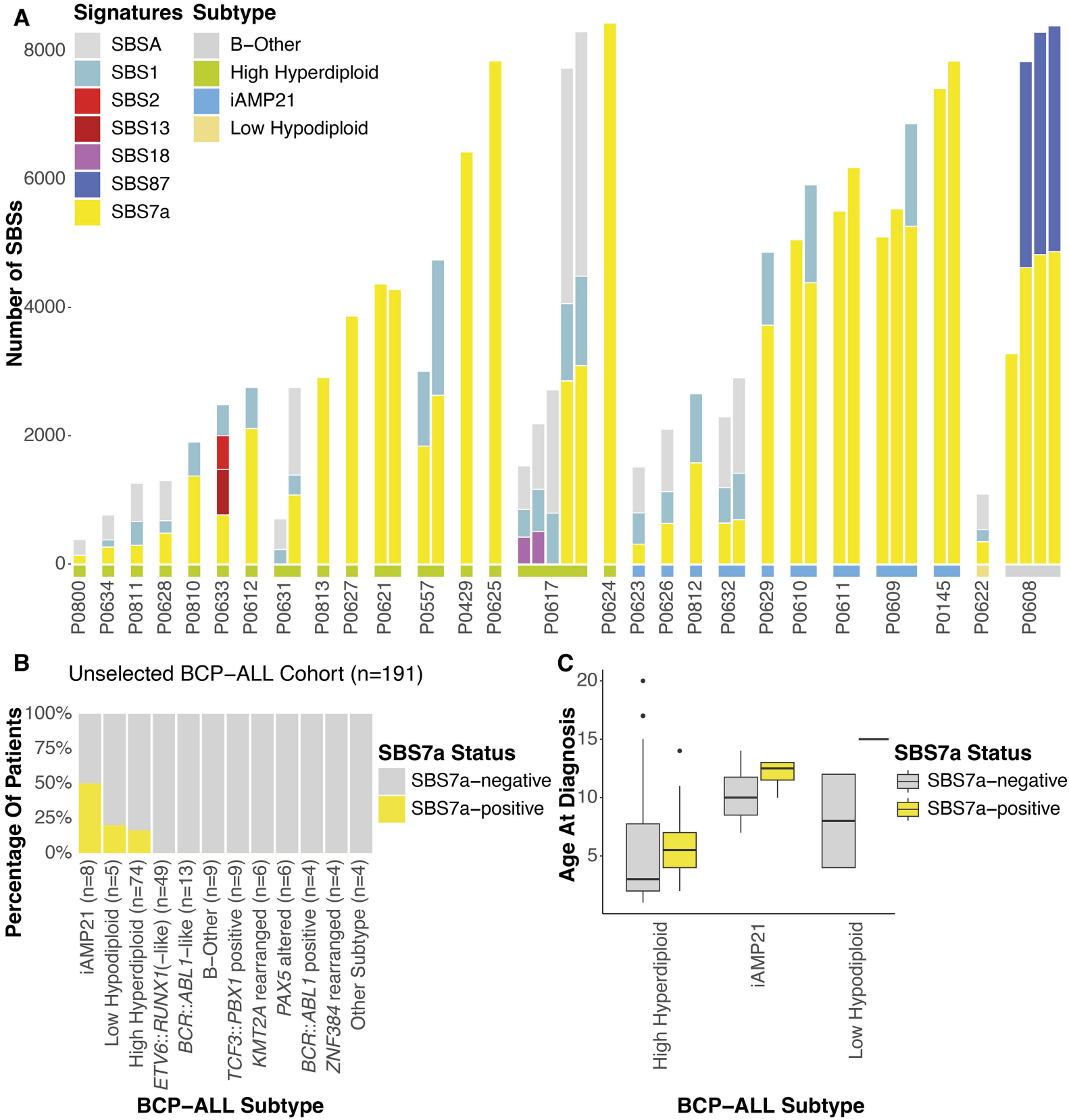
A
Signatures
SBSA
SBS1
SBS2
SBS13
SBS18
SBS87
SBS7a
Subtype
B–Other
High Hyperdiploid
iAMP21
Low Hypodiploid
Number of SBSs
8000
6000
4000
2000
0
P0800
P0634
P0811
P0628
P0810
P0633
P0612
P0631
P0813
P0627
P0621
P0557
P0429
P0625
P0617
P0624
P0623
P0626
P0812
P0632
P0629
P0610
P0611
P0609
P0145
P0622
P0608
B
Unselected BCP–ALL Cohort (n=191)
Percentage Of Patients
100%
75%
50%
25%
0%
SBS7a Status
SBS7a–negative
SBS7a–positive
iAMP21 (n=8)
Low Hypodiploid (n=5)
High Hyperdiploid (n=74)
ETV6::RUNX1(–like) (n=49)
BCR::ABL1–like (n=13)
B–Other (n=9)
TCF3::PBX1 positive (n=9)
KMT2A rearranged (n=6)
PAX5 altered (n=6)
BCR::ABL1 positive (n=4)
ZNF384 rearranged (n=4)
Other Subtype (n=4)
BCP–ALL Subtype
C
Age At Diagnosis
20
15
10
5
SBS7a Status
SBS7a–negative
SBS7a–positive
High Hyperdiploid
iAMP21
Low Hypodiploid
BCP–ALL Subtype

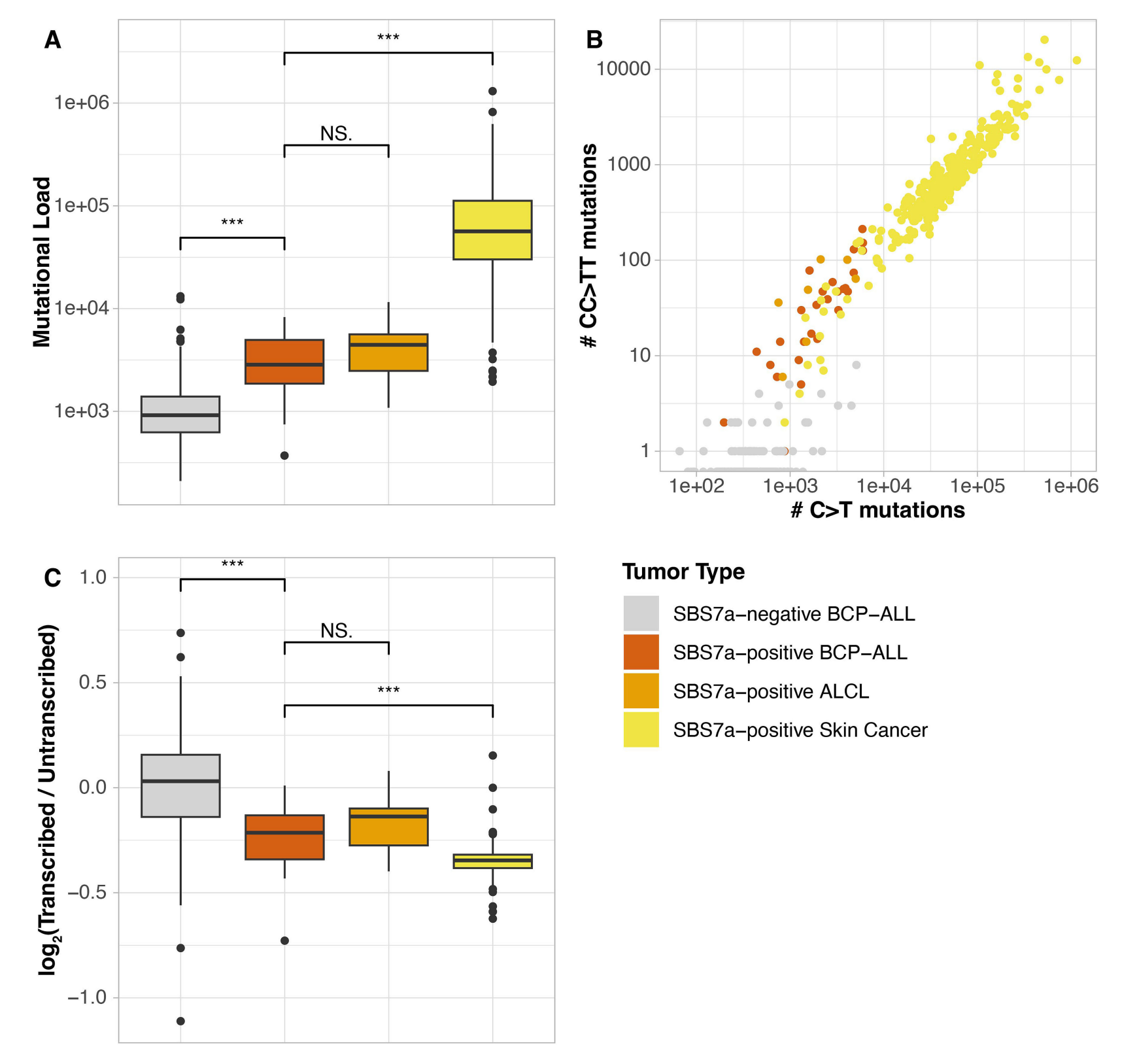
A
Mutational Load
1e+06
1e+05
1e+04
1e+03
***
NS.
***
B
CC>TT mutations
10000
1000
100
10
1
1e+02
1e+03
1e+04
1e+05
1e+06
C>T mutations
C
log2(Transcribed / Untranscribed)
1.0
0.5
0.0
−0.5
−1.0
***
NS.
***
Tumor Type
SBS7a−negative BCP−ALL
SBS7a−positive BCP−ALL
SBS7a−positive ALCL
SBS7a−positive Skin Cancer

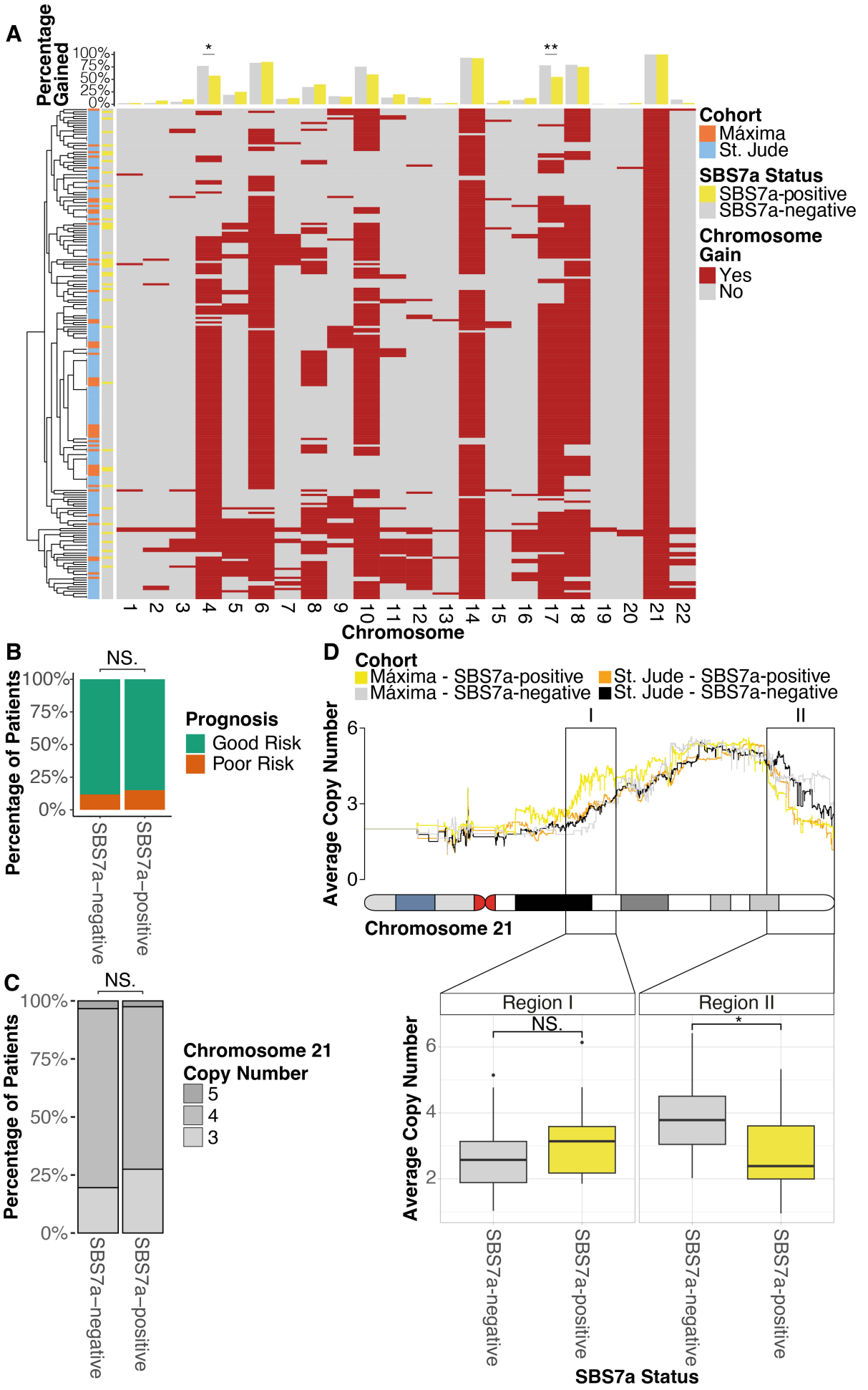
A
Percentage Gained
100%
75%
50%
25%
0%
*
**
Cohort
Máxima
St. Jude
SBS7a Status
SBS7a-positive
SBS7a-negative
Chromosome Gain
Yes
No
1 2 3 4 5 6 7 8 9 10 11 12 13 14 15 16 17 18 19 20 21 22
Chromosome
B
NS.
Percentage of Patients
100%
75%
50%
25%
0%
Prognosis
Good Risk
Poor Risk
SBS7a−negative
SBS7a−positive
C
NS.
Percentage of Patients
100%
75%
50%
25%
0%
Chromosome 21 Copy Number
5
4
3
SBS7a−negative
SBS7a−positive
D
Cohort
Máxima - SBS7a-positive
St. Jude - SBS7a-positive
Máxima - SBS7a-negative
St. Jude - SBS7a-negative
I
II
Average Copy Number
6
3
0
Chromosome 21
Region I
Region II
NS.
*
Average Copy Number
6
4
2
SBS7a-negative
SBS7a-positive
SBS7a-negative
SBS7a-positive
SBS7a Status

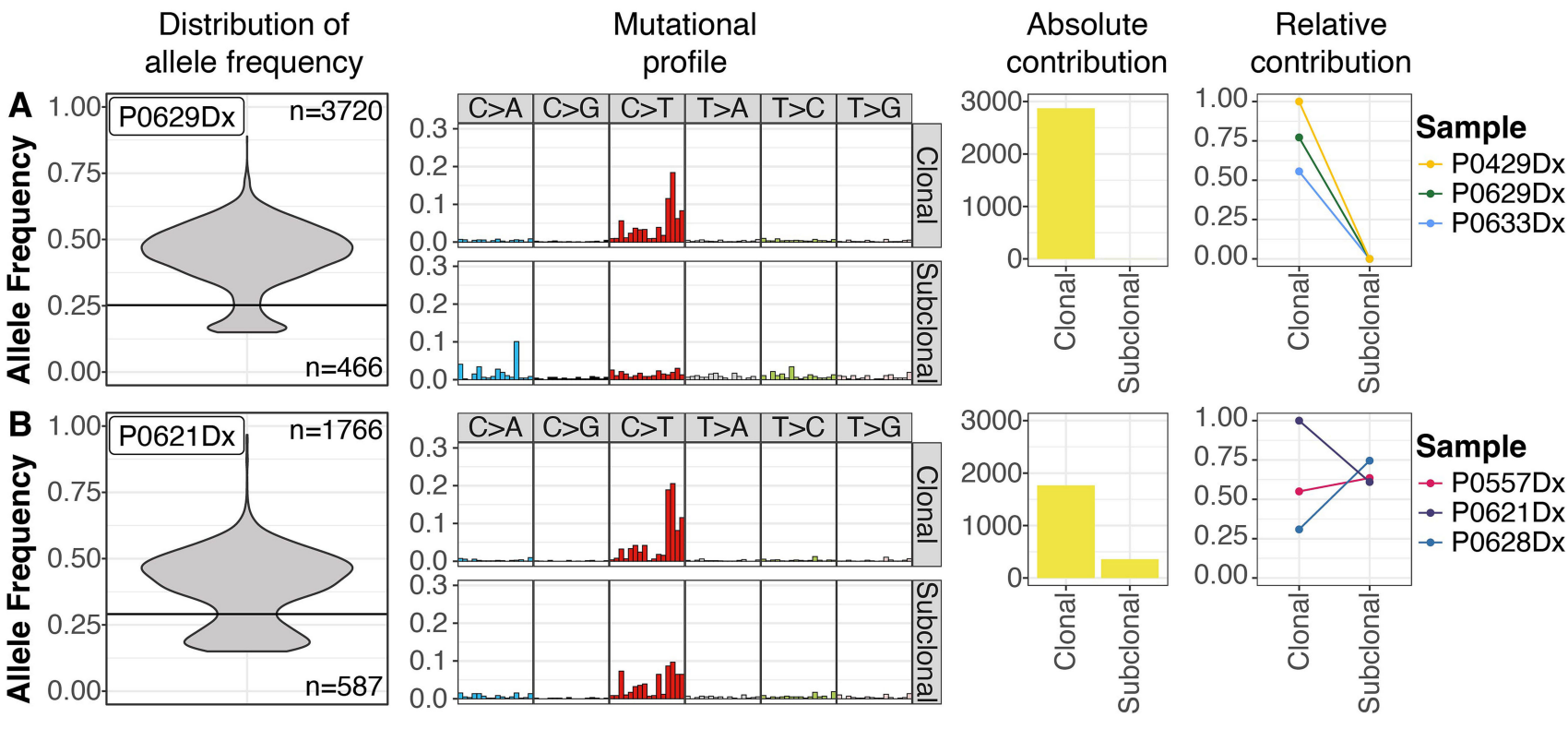
Distribution of allele frequency
Mutational profile
Absolute contribution
Relative contribution
A
B
Allele Frequency
P0629Dx
n=3720
n=466
P0621Dx
n=1766
n=587
C>A
C>G
C>T
T>A
T>C
T>G
Clonal
Subclonal
Sample
P0429Dx
P0629Dx
P0633Dx
P0557Dx
P0621Dx
P0628Dx

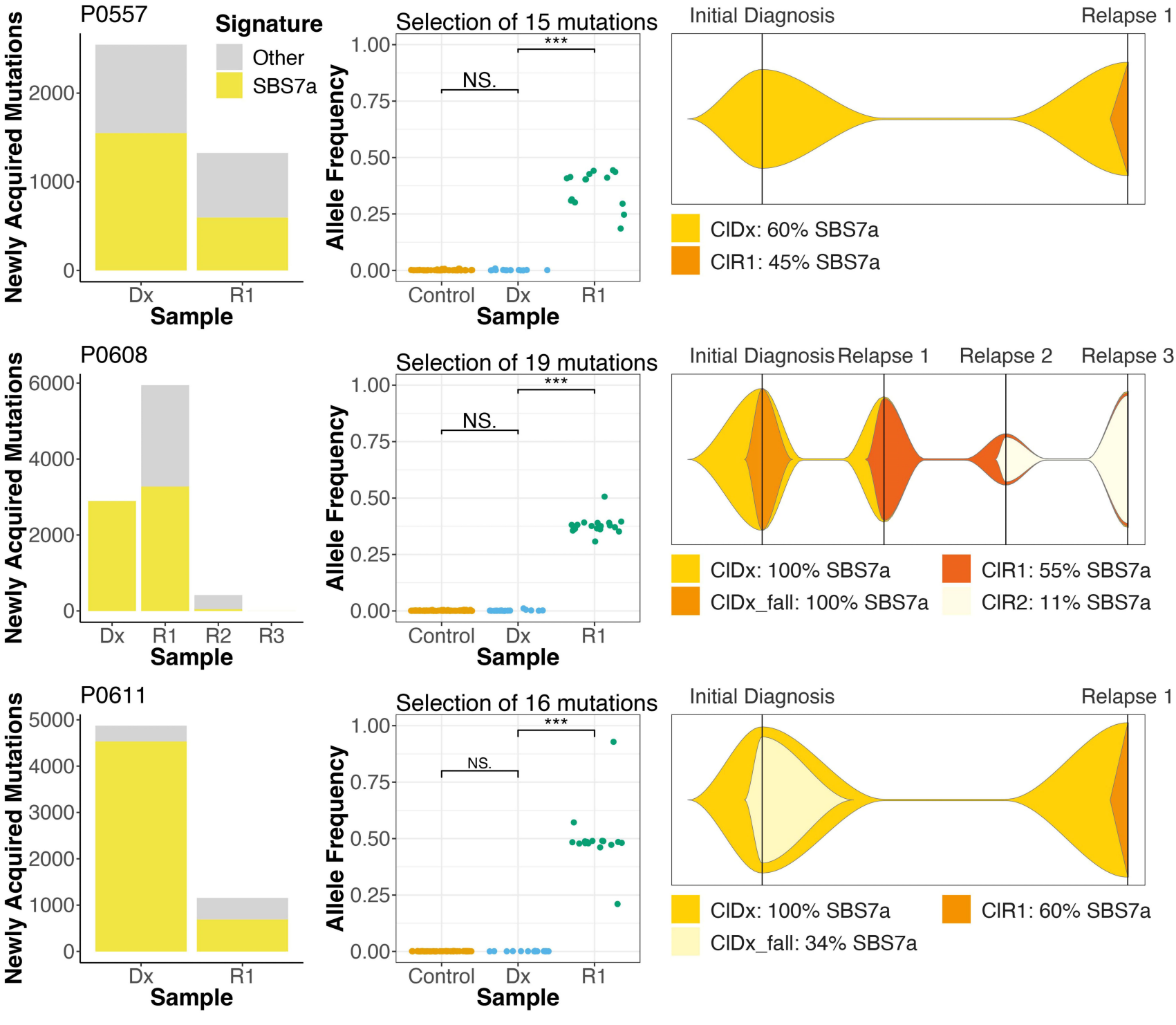
P0557
Signature
Other
SBS7a
Newly Acquired Mutations
2000
1000
0
Dx
R1
Sample
Selection of 15 mutations
Allele Frequency
1.00
0.75
0.50
0.25
0.00
***
NS.
Control
Dx
R1
Sample
Initial Diagnosis
Relapse 1
ClDx: 60% SBS7a
ClR1: 45% SBS7a
P0608
Newly Acquired Mutations
6000
4000
2000
0
Dx
R1
R2
R3
Sample
Selection of 19 mutations
Allele Frequency
1.00
0.75
0.50
0.25
0.00
***
NS.
Control
Dx
R1
Sample
Initial Diagnosis
Relapse 1
Relapse 2
Relapse 3
ClDx: 100% SBS7a
ClDx_fall: 100% SBS7a
ClR1: 55% SBS7a
ClR2: 11% SBS7a
P0611
Newly Acquired Mutations
5000
4000
3000
2000
1000
0
Dx
R1
Sample
Selection of 16 mutations
Allele Frequency
1.00
0.75
0.50
0.25
0.00
***
NS.
Control
Dx
R1
Sample
Initial Diagnosis
Relapse 1
ClDx: 100% SBS7a
ClDx_fall: 34% SBS7a
ClR1: 60% SBS7a

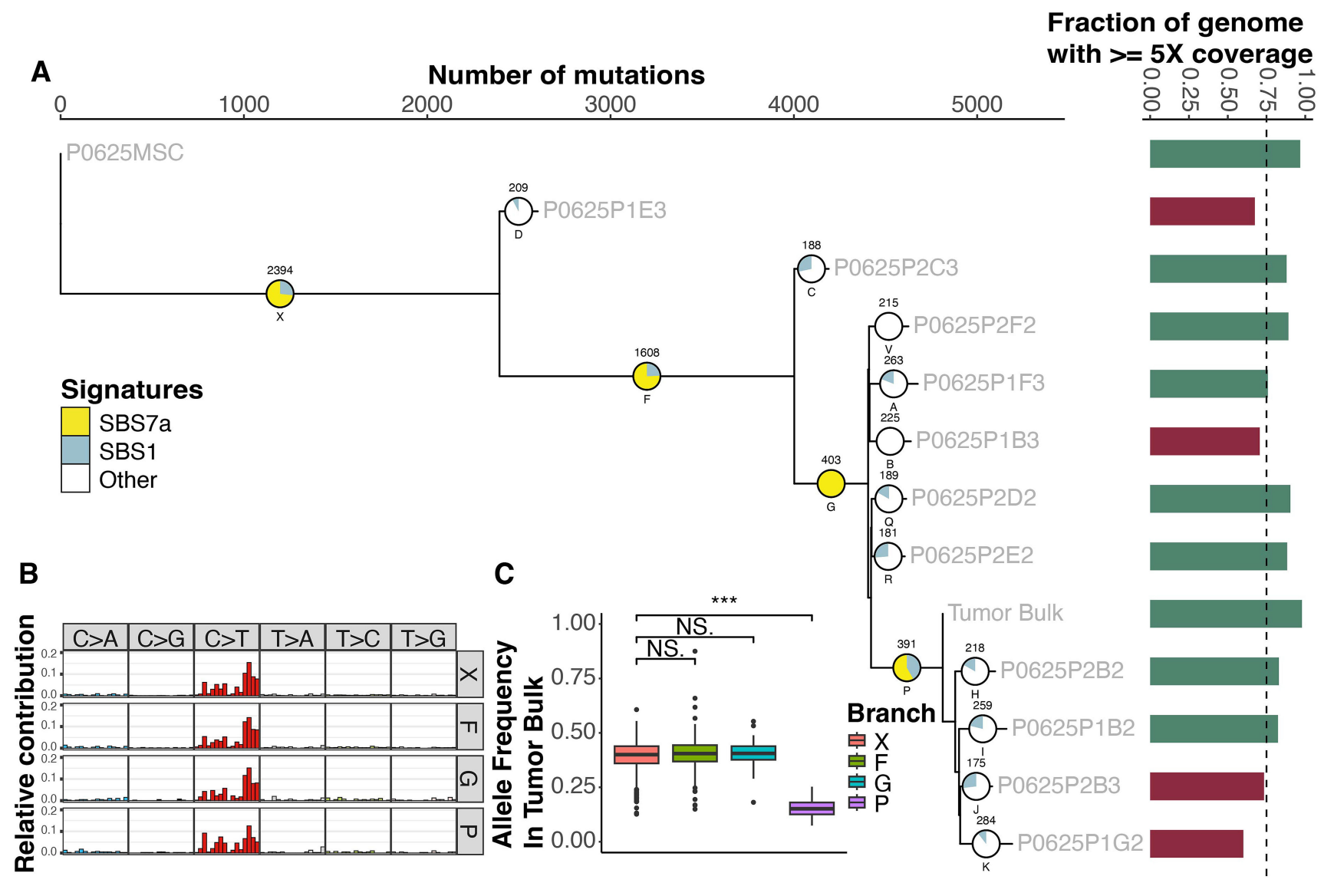
A
Number of mutations
0
1000
2000
3000
4000
5000
Fraction of genome with >= 5X coverage
0.00
0.25
0.50
0.75
1.00
P0625MSC
209
D
P0625P1E3
2394
X
188
C
P0625P2C3
215
V
P0625P2F2
1608
F
263
A
P0625P1F3
225
B
P0625P1B3
403
G
189
Q
P0625P2D2
181
R
P0625P2E2
Tumor Bulk
391
P
218
H
P0625P2B2
259
I
P0625P1B2
175
J
P0625P2B3
284
K
P0625P1G2
Signatures
SBS7a
SBS1
Other
B
Relative contribution
C>A
C>G
C>T
T>A
T>C
T>G
X
F
G
P
C
Allele Frequency In Tumor Bulk
1.00
0.75
0.50
0.25
0.00
***
NS.
NS.
Branch
X
F
G
P

UV-induced mutations accumulate during early clonal expansion in aneuploid subtypes of pediatric B-cell precursor acute lymphoblastic leukemia

Table of contents

Supplementary Table S9: Mean number of gained chromosomes in SBS7a-positive and SBS7a-negative hyperdiploid B-ALL

Supplementary tables can be found in the Supplementary Excel Table.

Supplementary methods

Reference and validation cohorts

We received a pan-cancer pediatric WGS cohort and a BCP-ALL RNAseq cohort from the Princess Máxima Center biobank (PMCLAB2021.279 & PMCLAB2022.343). RNA and DNA were isolated automatically using the Allprep DNA/RNA/miRNA Universal Kit (Qiagen, 80224) and the QIAcube Connect (Qiagen, 9002864). Library prep for WGS was performed automatically using 150 ng DNA, the KAPA HyperPlus Kit (Roche, 07962428001) and the epMotion 5075 (Eppendorf, 12018865). Library prep for RNAseq was performed manually using 300 ng RNA and the KAPA RNA HyperPrep kit with RiboErase (Roche, 08098140702). Subsequent sequencing was performed on Illumina Novaseq 6000 (Illumina) to generate 150 base-pair paired-end reads.

As an additional validation cohort we used RNAseq and WGS data of high hyperdiploid and iAMP21 BCP-ALL samples from St. Jude Children's Research Hospital in Memphis, Philadelphia, which we requested through the St. Jude Cloud.[1] The relative contributions of mutational signatures were either used as reported in literature,[2] or extracted with the same methods used for in-house data. A small subset of the RNAseq data was generated using unstranded instead of stranded RNAseq. Calling of overlapping genes is greatly improved in stranded RNAseq compared to unstranded RNAseq, causing significant bias.[3] As such we excluded the two unstranded RNAseq high hyperdiploid BCP-ALL samples and analyzed the unstranded (n=15) and stranded (n=12) RNAseq iAMP21 BCP-ALL samples separately.

WGS data analysis

Reads generated by WGS were mapped to the GRCh38 human reference genome using the Burrows-Wheeler Aligner (BWA) v0.7.13.[4] Picard v2.20.1[5] was used to mark duplicate reads, followed by base quality score recalibration using Genome Analysis ToolKit (GATK) v4.0.1.2.[6] Somatic mutations were called using Mutect2 from GATK v4.1.1.0 and annotated using Variant Effect Predictor v105.[7] R v4.1.2 was used to filter out mutations overlapping with centromeric regions or with a population frequency above 1% according to either gnomAD v3.0[8] or GoNL.[9] Mutations were kept if they were supported by 5 alternative reads at an allele frequency of at least 0.15 and a minimum coverage of 20.

Comparison with SBS7a-positive skin cancer

Somatic data for a cohort of adult metastatic skin cancers were received from the Hartwig Medical Foundation,[10] and further filtered with the same methods used for in-house data. To determine the mutational load, the total number of SBSs was calculated. The number of CC>TT mutations was determined using MutationalPatterns v3.4.1.[11] Transcriptional strand bias was calculated using MutationalPatterns v3.4.1 and the known genes table from UCSC for hg38.[11,12]

RNA expression analysis

Reads generated by RNA sequencing were mapped to GRCh38 (gencode version 31) using STAR v2.7.2d,[13] after which count matrices were generated with Rsubread v1.6.4.[14] Further analysis was performed using DESeq2 v.1.34.0.[15] For each dataset, genes without any counts were removed. For NER pathway analysis, counts were transformed using Variance Stabilizing Transformation, genes in the NER pathway in the Kyoto Encyclopedia of Genes and Genomes were selected and the deviation from the average per gene was calculated. Heatmaps were generated using pheatmap v1.0.12.[16] Differential expression analysis was

performed with DESeq2, comparing SBS7a-positive to SBS7a-negative samples and correcting for sex as a confounder. An adjusted *P*-value of 0.05 was used as a threshold to identify differentially expressed genes. Volcano plots were made using EnhancedVolcano v1.12.0.[17]
For subtype comparisons, 10 samples of iAMP21 BCP-ALL and 72 samples of high hyperdiploid BCP-ALL were separately compared to 58 cases of *ETV6*::*RUNX1*-positive or *ETV6*::*RUNX1*-like BCP-ALL. For gene set enrichment analysis, genes were ordered on log2 fold change, and gene set enrichment analysis was performed on GO terms using clusterProfiler v4.2.2. Differentially expressed genes in both subtypes were identified using DESeq2 v1.34.0, using a *P*-value cutoff of 0.05 and a log2 fold change cutoff of 1 for upregulated and -1 for downregulated genes. Over-representation analysis of GO terms on the overlapping differentially expressed genes was performed using clusterProfiler v4.2.2.

Copy number analysis
Copy number alterations were called according to the GATK best practices, using GATK v4.1.7.0 and an in-house panel of normals. To study the timing of SBS7a, we selected somatic mutations on chromosome 21 with an allele frequency of at least 0.1. As a control, we called germline mutations on chromosome 21 using HaplotypeCaller and selected mutations with an allele frequency between 0.25 and 0.75 in the germline and an allele frequency of at least 0.1 in the tumor. Somatic and germline mutations overlapping with gained regions were selected with R v4.1.2. Karyotypes for patients with high hyperdiploid BCP-ALL were determined manually based on the CNA plots. Karyotype plots were generated using pheatmap v1.0.12[16] and samples were clustered using hierarchical clustering with complete linkage and euclidean distance. Prognostic risk group of high hyperdiploid patients was determined according to criteria identified by Enshaei et al[18]. For patients with iAMP21 BCP-ALL, segment files were used to visualize copy numbers with karyoploteR v1.20.3.[19]

Subclonal mutations
Mutations on amplified chromosomes were filtered out for analysis of subclones. Peaks in the allele frequency (AF) were identified using LaplacesDemon v16.1.6.[20] The minimum between these peaks was found using base R v4.1.2, and used as threshold between clonal and subclonal mutations. Tumors with a bimodal distribution and at least 200 subclonal mutations were selected for further inspection. For two patients, where the allele frequencies of the clonal and subclonal mutations showed great overlap, manual thresholds were applied to identify clonal and subclonal mutations.

Analysis of acquired mutations
SBSs were clustered based on their allele frequency dynamics over time,[21] and a refit with the previously identified mutational signatures for BCP-ALL was performed on the clusters. Based on these clusters, fishplots were generated using fishplot v0.5.1.[22]

Amplicon sequencing
We selected relapse-specific mutations, based on WGS data, that were likely caused by SBS7a using R v4.1.2 and the method described by Morganella et al, 2016 and Brady et al, 2019.[23,24] We then excluded mutations in repeat-rich regions and aimed to include at least 15 mutations per patient, preferably in coding regions. We designed primers for 300-400 bp

fragments using primer3[25] and included 15 mutations for P0557, 19 mutations for P0608 and 16 mutations for P0611. Each primer pair was first validated separately and then multiplexed in sets of three and one set of two, for a total of 17 pools, and validated again. Multiplex PCR was then performed using Taq polymerase (Roche, 11647679001) with an initial 2 minutes at 94°C, followed by 35 cycles of 30s at 94°C, 45s at 60°C and 60s at 72°C, then finalized with 7 minutes at 72°C. 150 ng DNA was used for initial diagnosis samples and 50 ng DNA was used for relapse samples. Successful fragment amplification was confirmed using gel electrophoresis. Samples were purified using AMPure XPbeads (Beckmann Coulter, B37419AB), and DNA concentration was measured using the Qubit dsDNA Quantitation High Sensitivity kit (Thermo Fisher, Q32854) and Qubit™ 4 Fluorometer (Thermo Fisher, Q33238).

Illumina DNA Prep (Illumina, 20015826) and Nextera DNA CD Indexes (24 indexes, 24 samples) (Illumina, 20015881) were used for library prep. PCR amplicons of each sample were pooled in one library, i.e. the 17 multiplex PCR amplicons generated for the initial diagnosis of P0557 were pooled in one library. The six resulting libraries were then pooled, with initial diagnosis samples and relapse samples in a 3:1 ratio. sequencing was performed on the Illumina iSeq 100 (Illumina, 20021532) with the iSeq 100 i1 Reagent v2 (300-cycle) (Illumina, 20031371) for 2 x 150 bp paired-end reads.
BWA v0.7.13 was used to map the resulting reads to the GRCh38 human reference genome. The number of reads supporting each allele for the selected positions was extracted using bam-readcount v0.8.[26] As all 50 mutations were sequenced in all samples, the samples that did not carry a mutation could serve as a negative control for the sample that did carry said mutation.

Mutational driver analysis
Clustered mutations which are either exonic or affect splicing were filtered for a CADD score of at least 20, and mutations were selected based on a list of known ALL driver genes.[21] Using the relative contributions per cluster, the probability of each mutation being caused by SBS7a was calculated based on the mutation type.[2,21,23] Mutations are shown which have a trinucleotide context which is also present in SBS7a and have a predicted probability to be caused by SBS7a of at least 50%.

Single-cell WGS data analysis
Reads were aligned to the GRCh38 human reference genome using BWA-MEM v2.2.1,[27] and duplicates were marked using GATK v4.4.0.0.[6] Mutations were called using GATK's HaplotypeCaller v4.4.0.0 and filtered using PTATO v1.3.3.[28] Mutations that, in one or more cells, had not been flagged as artifact by PTATO, had at least 5 supporting reads, had an allele frequency of at least 0.25 and had a mapping quality of at least 59, were used as positions for variant calling in all cells, the MSCs and the tumor bulk sample to ensure a minimal retention of artifacts. Variant calling was performed using Haplotypecaller and GenotypeGVCFs from GATK 4.2.0.0,[6] and SBSs were selected using bcftools v1.17.[29] An in-house blacklist of PTA artifacts, defined by a presence in multiple unrelated patients, was used to further filter the mutations. Lineage trees were constructed from the resulting mutations using CellPhyWrapper and visualized using CellPhyWrapperPlotting.[30,31] A refit using the previously identified signatures for BCP-ALL and the known PTA artifact signature was performed to obtain signature contributions for each branch that contained at least 100 mutations.

Supplementary References

1. McLeod C, Gout AM, Zhou X, et al. St. Jude Cloud: A Pediatric Cancer Genomic Data-Sharing Ecosystem. Cancer Discov 2021;11(5):1082–1099.
2. Brady SW, Roberts KG, Gu Z, et al. The genomic landscape of pediatric acute lymphoblastic leukemia. Nat Genet 2022;54(9):1376–1389.
3. Zhao S, Zhang Y, Gordon W, et al. Comparison of stranded and non-stranded RNA-seq transcriptome profiling and investigation of gene overlap. BMC Genomics 2015;16(1):675.
4. Li H, Durbin R. Fast and accurate short read alignment with Burrows-Wheeler transform. Bioinformatics 2009;25(14):1754–1760.
5. Picard. http://broadinstitute.github.io/picard/ (accessed June 12, 2025).
6. Van der Auwera GA, O'Connor BD. Genomics in the Cloud: Using Docker, GATK, and WDL in Terra. "O'Reilly Media, Inc."; 2020. 496 p.
7. McLaren W, Gil L, Hunt SE, et al. The Ensembl Variant Effect Predictor. Genome Biol 2016;17(1):122.
8. Chen S, Francioli LC, Goodrich JK, et al. A genomic mutational constraint map using variation in 76,156 human genomes. Nature 2024;625(7993):92–100.
9. Boomsma DI, Wijmenga C, Slagboom EP, et al. The Genome of the Netherlands: design, and project goals. Eur J Hum Genet 2014;22(2):221–227.
10. Priestley P, Baber J, Lolkema MP, et al. Pan-cancer whole-genome analyses of metastatic solid tumours. Nature 2019;575(7781):210–216.
11. Manders F, Brandsma AM, de Kanter J, et al. MutationalPatterns: the one stop shop for the analysis of mutational processes. BMC Genomics 2022;23(1):134.
12. Perez G, Barber GP, Benet-Pages A, et al. The UCSC Genome Browser database: 2025 update. Nucleic Acids Res 2025;53(D1):D1243–D1249.
13. Dobin A, Davis CA, Schlesinger F, et al. STAR: ultrafast universal RNA-seq aligner. Bioinformatics 2013;29(1):15–21.
14. Liao Y, Smyth GK, Shi W. The R package Rsubread is easier, faster, cheaper and better for alignment and quantification of RNA sequencing reads. Nucleic Acids Res 2019;47(8):e47.
15. Love MI, Huber W, Anders S. Moderated estimation of fold change and dispersion for RNA-seq data with DESeq2. *bioRxiv*.
16. Kolde R. pheatmap: Pretty Heatmaps. *R package version 1.0.12*. https://github.com/raivokolde/pheatmap (2025).
17. Blighe K, Rana S, Lewis M. EnhancedVolcano: Publication-ready volcano plots with enhanced colouring and labeling. *R package version 1.12.0*. https://bioconductor.org/packages/EnhancedVolcano (2025).
18. Enshaei A, Vora A, Harrison CJ, Moppett J, Moorman AV. Defining low-risk high hyperdiploidy in patients with paediatric acute lymphoblastic leukaemia: a retrospective analysis of data from the UKALL97/99 and UKALL2003 clinical trials. Lancet Haematol 2021;8(11):e828–e839.
19. Gel B, Serra E. karyoploteR: an R/Bioconductor package to plot customizable genomes displaying arbitrary data. Bioinformatics 2017;33(19):3088–3090.
20. Statisticat, LLC. LaplacesDemon: Complete Environment for Bayesian Inference. *R package version 16.1.6*. https://web.archive.org/web/20150206004624/http://www.bayesian-inference.com/software (2021).

21. van der Ham CG, Suurenbroek LC, Kleisman MM, et al. Mutational mechanisms in multiply relapsed pediatric acute lymphoblastic leukemia. Leukemia 2024;38(11):2366–2375.
22. Miller CA, McMichael J, Dang HX, et al. Visualizing tumor evolution with the fishplot package for R. BMC Genomics 2016;17(1):880.
23. Morganella S, Alexandrov LB, Glodzik D, et al. The topography of mutational processes in breast cancer genomes. Nat Commun 2016;7(1):11383.
24. Brady SW, Ma X, Bahrami A, et al. The clonal evolution of metastatic osteosarcoma as shaped by cisplatin treatment. Mol Cancer Res 2019;17(4):895–906.
25. Kõressaar T, Lepamets M, Kaplinski L, Raime K, Andreson R, Remm M. Primer3_masker: integrating masking of template sequence with primer design software. Bioinformatics 2018;34(11):1937–1938.
26. Khanna A, Larson DE, Srivatsan SN, et al. Bam-readcount - rapid generation of basepair-resolution sequence metrics. ArXiv 2021;7(69):3722.
27. Vasimuddin M, Misra S, Li H, Aluru S. Efficient architecture-aware acceleration of BWA-MEM for multicore systems. In: 2019 IEEE International Parallel and Distributed Processing Symposium (IPDPS). IEEE; p.
28. Middelkamp S, Manders F, Peci F, et al. Comprehensive single-cell genome analysis at nucleotide resolution using the PTA Analysis Toolbox. Cell Genom 2023;3(9):100389.
29. Danecek P, Bonfield JK, Liddle J, et al. Twelve years of SAMtools and BCFtools. Gigascience;10(2):.
30. Bertrums EJM, de Kanter JK, Derks LLM, et al. Selective pressures of platinum compounds shape the evolution of therapy-related myeloid neoplasms. Nat Commun 2024;15(1):6025.
31. Kozlov A, Alves JM, Stamatakis A, Posada D. CellPhy: accurate and fast probabilistic inference of single-cell phylogenies from scDNA-seq data. Genome Biol 2022;23(1):37.

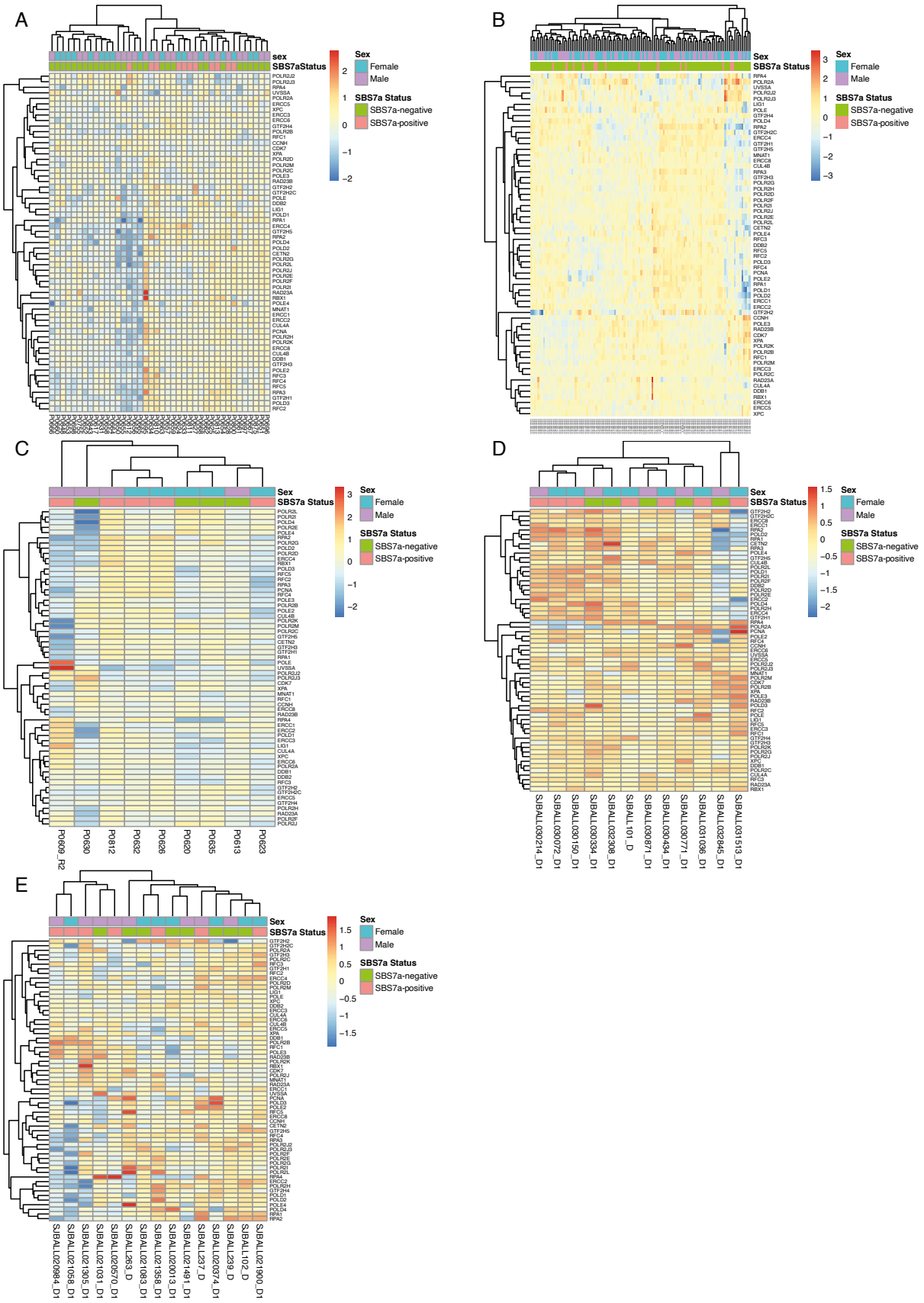

Supplementary figure S1. Genes in the NER pathway show no differential expression between SBS7a-positive and SBS7a-negative BCP-ALL. Whereas the NER pathway is upregulated in high hyperdiploid BCP-ALL in the cohort from the Princess Máxima Center (A), this is not seen in the high hyperdiploid BCP-ALL dataset from St. Jude (B), or in iAMP21

BCP-ALL, as seen in the cohort from the Princess Máxima Center (C) and the stranded (D) and unstranded (E) cohort from St. Jude. A-E) Heatmaps of differentially expressed genes between SBS7a-positive and SBS7a-negative samples in different cohorts. Bars above the plot show sex and whether a sample is SBS7a-positive (red) or SBS7a-negative (green). All genes from the NER pathway according to the Kyoto Encyclopedia of Genes and Genomes (Table S5) with expression in at least one sample are shown on the y-axis, sample names are shown on the x-axis.

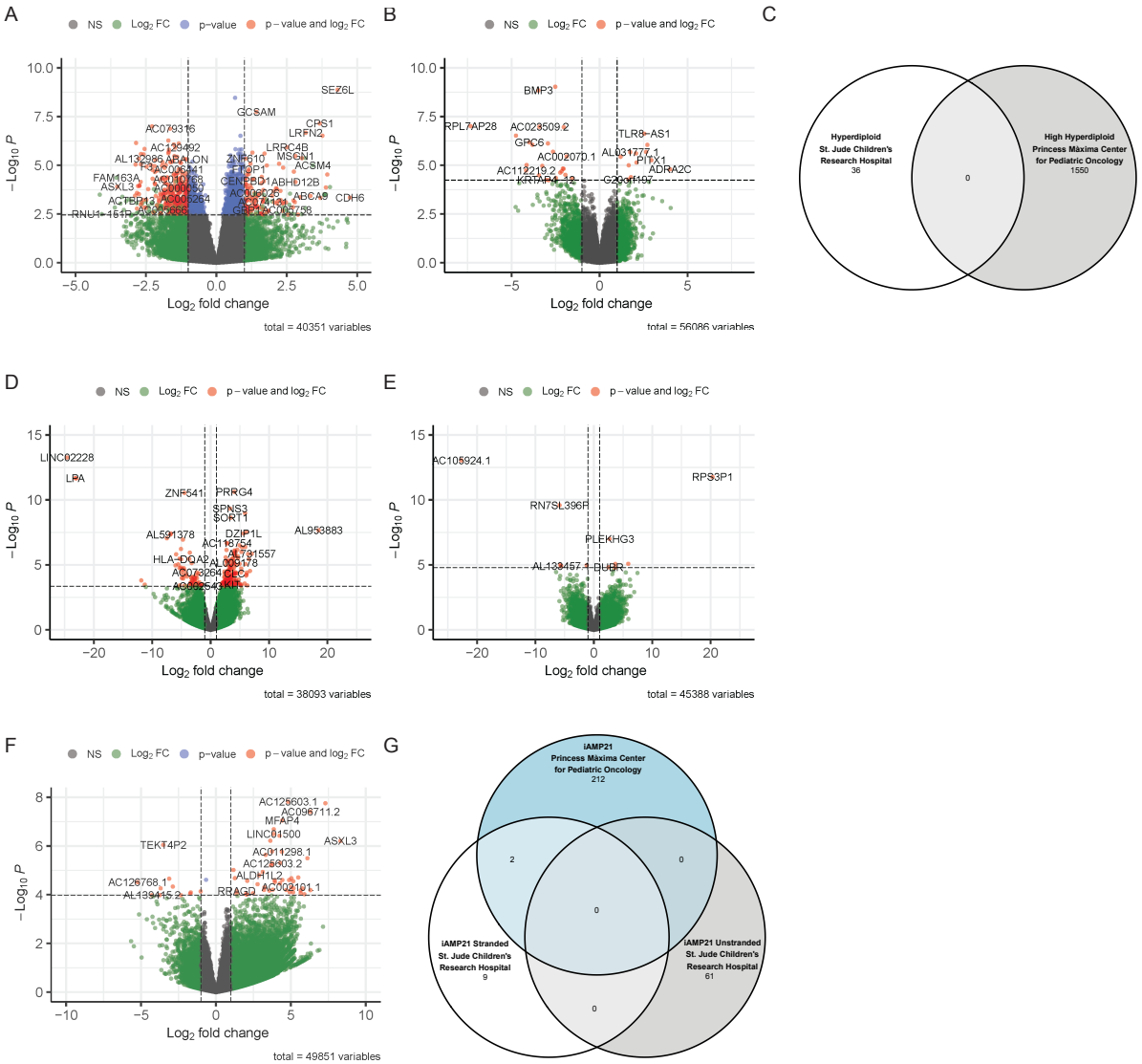

Supplementary figure S2. Differential expression analysis for samples with and without SBS7a. A-B) Volcano plots of differentially expressed genes in hyperdiploid samples with SBS7a compared to samples without SBS7a. The y-axis represents the -log10 adjusted *P*-value and the x-axis represents the log2 fold change. Each gene is plotted as a circle and highlighted in green if there is a significant log2 fold change, highlighted in blue if there is a significant adjusted *P*-value and highlighted in red if there is both a significant log2 fold change and a significant adjusted *P*-value. A) Volcano plot of differential expression analysis between SBS7a-positive and SBS7a-negative high hyperdiploid BCP-ALL samples collected at the Princess Maxima center for Pediatric Oncology. B) Volcano plot of differential expression analysis between SBS7a-positive and SBS7a-negative high hyperdiploid BCP-ALL of the validation cohort collected by St. Jude children's hospital. C) Venn diagram showing the overlap in differentially expressed genes detected in our high hyperdiploid BCP-ALL samples and the St. Jude children's hospital hyperdiploid BCP-ALL samples. D) Volcano plot of differential expression analysis between SBS7a-positive and SBS7a-negative iAMP21 BCP-ALL collected at the Princess Maxima center for Pediatric Oncology. E) Volcano plot of differential expression analysis between SBS7a-positive and SBS7a-negative iAMP21 BCP-ALL samples of the validation cohort collected by St. Jude children's hospital on which stranded RNAseq was performed. F) Volcano plot of differential expression analysis between SBS7a-positive and

SBS7a-negative iAMP21 BCP-ALL samples of the validation cohort collected by St. Jude children's hospital on which unstranded RNAseq was performed. G) Venn diagram showing the overlap in differentially expressed genes detected in our iAMP21 BCP-ALL samples, the St. Jude children's hospital iAMP21 BCP-ALL samples with stranded RNAseq data and the St. Jude children's hospital iAMP21 BCP-ALL samples with unstranded RNAseq data. The two upregulated genes detected in both iAMP21 cohorts are *TMEM40* and *ZSCAN23*, which encode a transmembrane protein and a transcription factor, respectively.

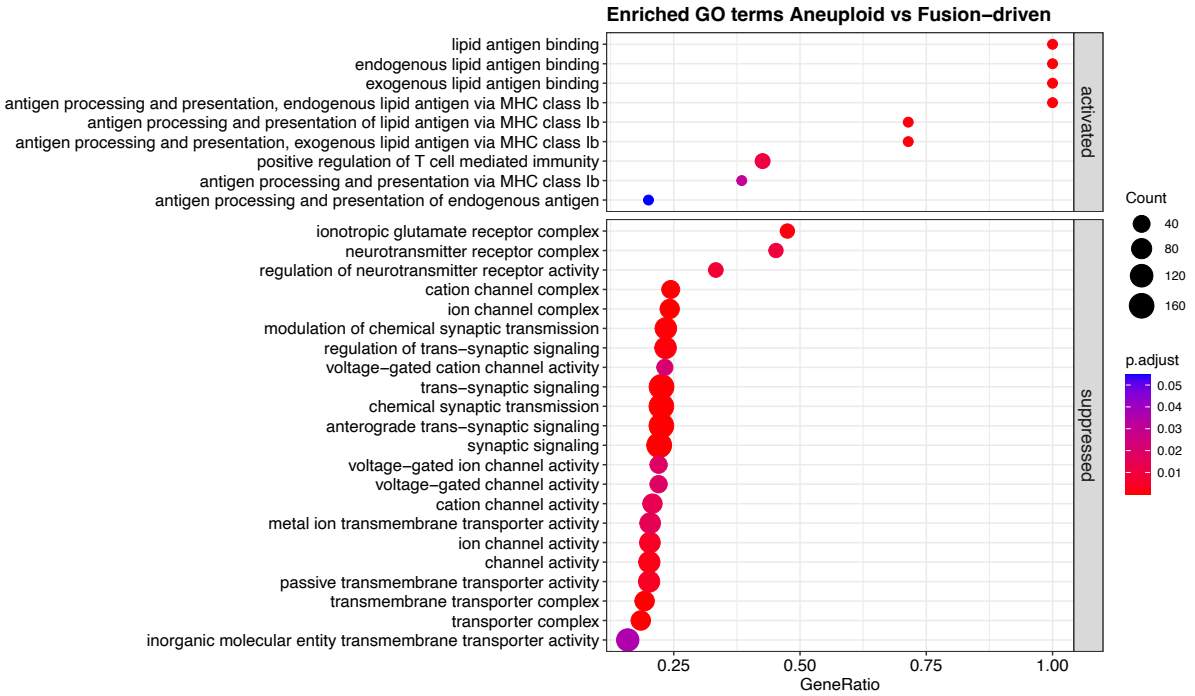

Supplementary figure S3. Gene set enrichment analysis comparing aneuploid BCP-ALL subtypes to *ETV6*::*RUNX1* BCP-ALL. Dotplot of gene sets which are enriched in both iAMP21 and high hyperdiploid BCP-ALL compared to *ETV6*::*RUNX1* BCP-ALL. None of the gene sets identified in this analysis are indicative of a higher tendency of aneuploid BCP-ALL subtypes to migrate.

Supplementary figure S4. Over-representation analysis of genes which are differentially expressed in both iAMP21 and high hyperdiploid BCP-ALL compared to *ETV6*::*RUNX1* BCP-ALL. Dotplots of the top-50 enriched GO terms in upregulated (A) and downregulated (B) genes in aneuploid (iAMP21 and high hyperdiploid) BCP-ALL compared to *ETV6*::*RUNX1* BCP-ALL are shown. GO terms associated with migration are indicated with red arrows and are all enriched in upregulated genes.

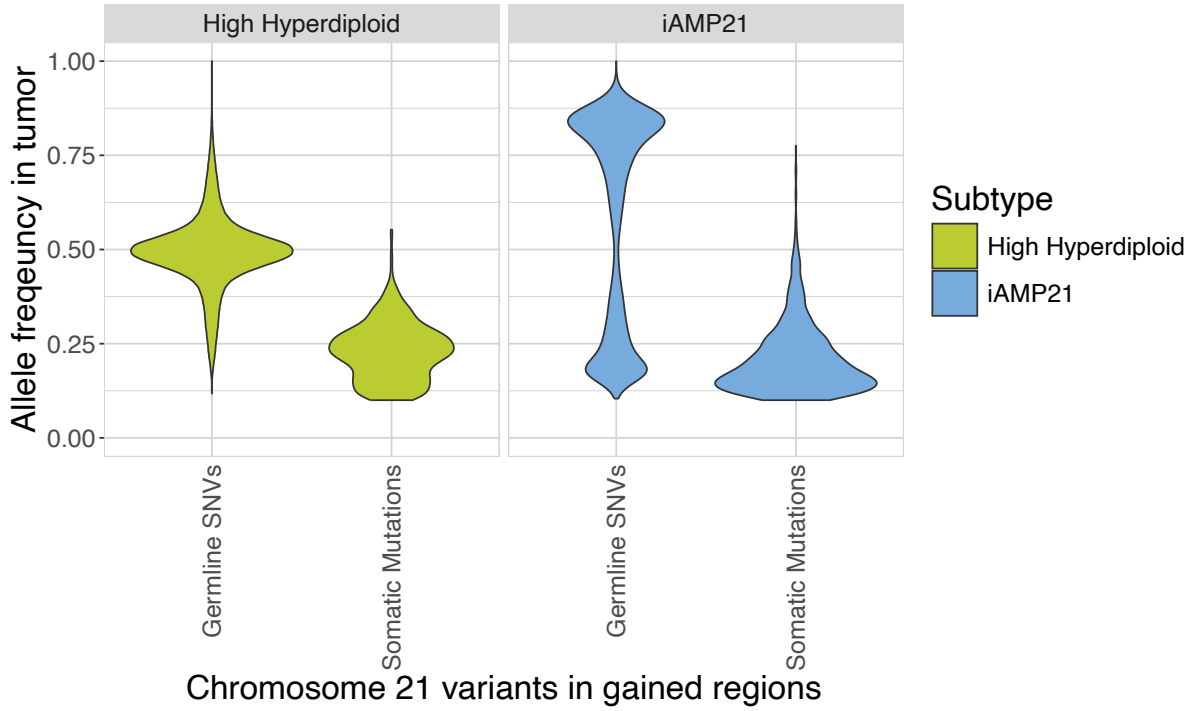

Supplementary figure S5. Somatic SBS7a-associated mutations are accumulated after chromosome 21 amplification in high hyperdiploid and iAMP21 BCP-ALL. Violin plots depicting the allele frequency of germline and somatic single base substitutions on chromosome 21 in high hyperdiploid (n=16) and iAMP21 BCP-ALL (n=9). In high hyperdiploid BCP-ALL, chromosome 21 typically has 4 copies, and germline SNVs of chromosome 21 therefore retain their allele frequency of 0.5. Somatic chromosome 21 mutations, however, present with an allele frequency of approximately 0.25, suggesting that they accumulated after amplification. Chromosome 21 in iAMP21 BCP-ALL has more complex CNAs, resulting in germline SNVs of chromosome 21 having either a high (~0.85) or a low (~0.15) allele frequency. Somatic mutations typically present with a low allele frequency, again confirming that they accumulated after the primary driver event.

Supplementary figure S6. The allele frequency of ten out of 25 SBS7a-positive tumors shows a bimodal distribution, of which six present with at least 200 subclonal mutations. Violin plots of the allele frequency of all somatic single base substitutions in the initial diagnosis sample of 25 SBS7a-positive BCP-ALL. Horizontal lines show the split between subclone and major clone. Tumors P0557Dx, P0628Dx, P0621Dx, P0633Dx, P0629Dx and P0429Dx show a bimodal distribution with a subclone containing at least 200 mutations, and were therefore included in further analyses (red box). Four other tumors show a bimodal distribution with a subclone of less than 200 mutations, and one tumor (P0626Dx) shows a trimodal distribution. The remaining 14 tumors show a unimodal distribution. P0632 and P0612 were excluded due to insufficient tumor purity.

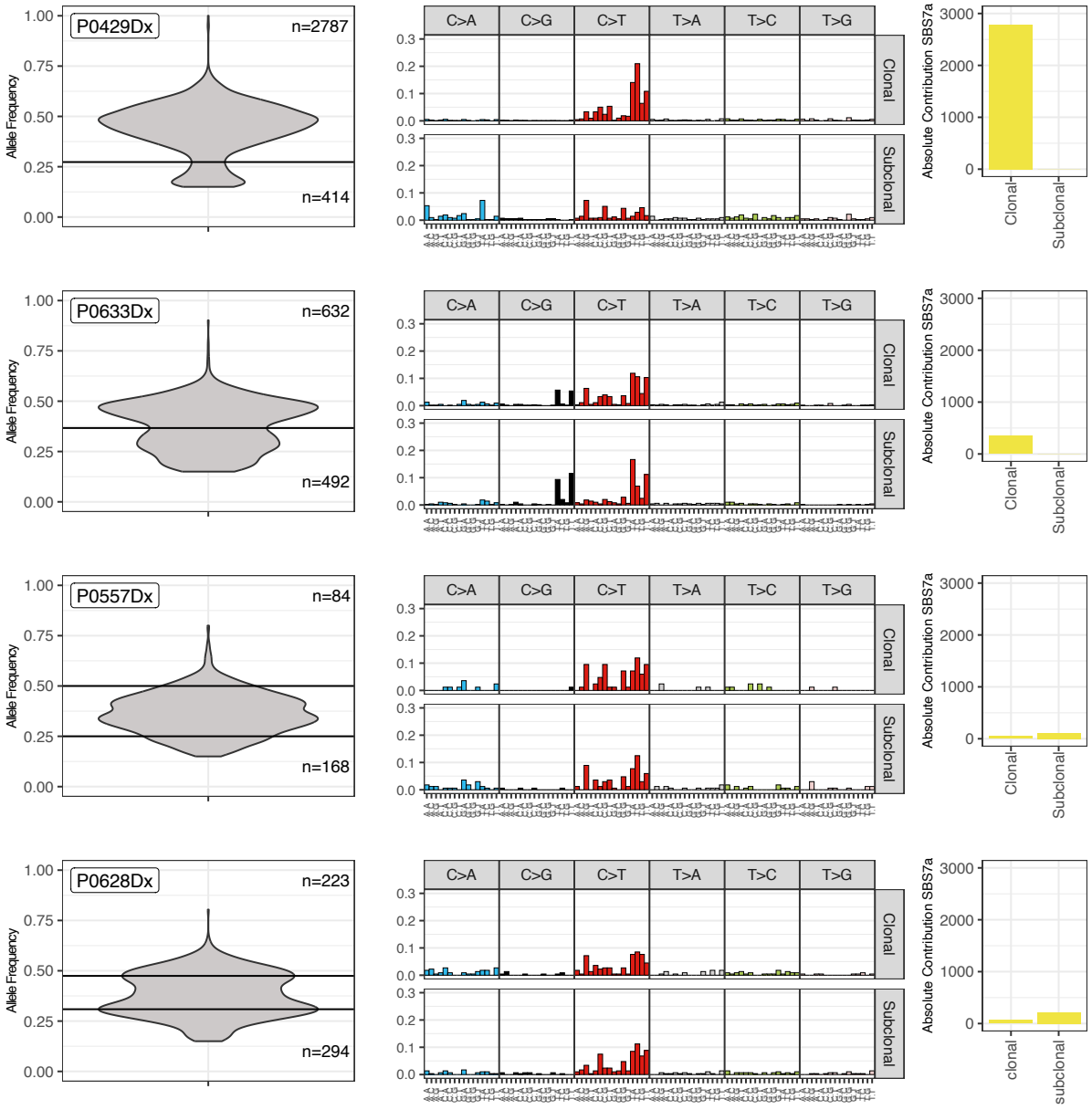

Supplementary figure S7. Sample P0429Dx and P0633Dx contain subclonal mutations without SBS7a, whereas samples P0557Dx and P0628Dx contain subclonal SBS7a-associated mutations. The first column depicts a violin plot of the allele frequency of somatic single base substitutions. Lines were added to indicate the split between mutations belonging to the major clone and subclonal mutations. The second column shows the mutational profile of the clonal and subclonal mutations as identified in the first column. The third column shows the relative contribution of SBS7a-associated mutations to the clonal and subclonal mutations identified in the first column.

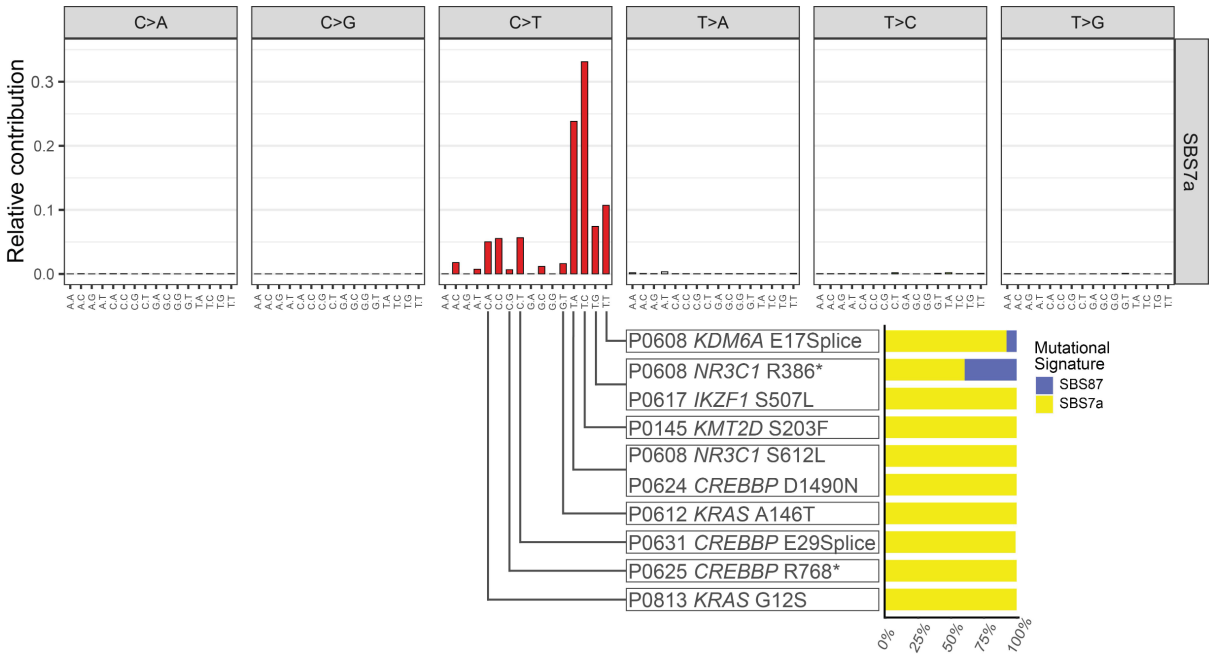

Supplementary figure S8. 10 mutations in driver genes have a high probability of being caused by SBS7a. COSMIC signature SBS7a is shown on top, with on the bottom potentially pathogenic mutations in known BCP-ALL driver or relapse-associated genes. Bar plots on the right show the probability of being caused by SBS7a (yellow) or SBS87 (purple) as calculated by *a posteriori* probability analysis.

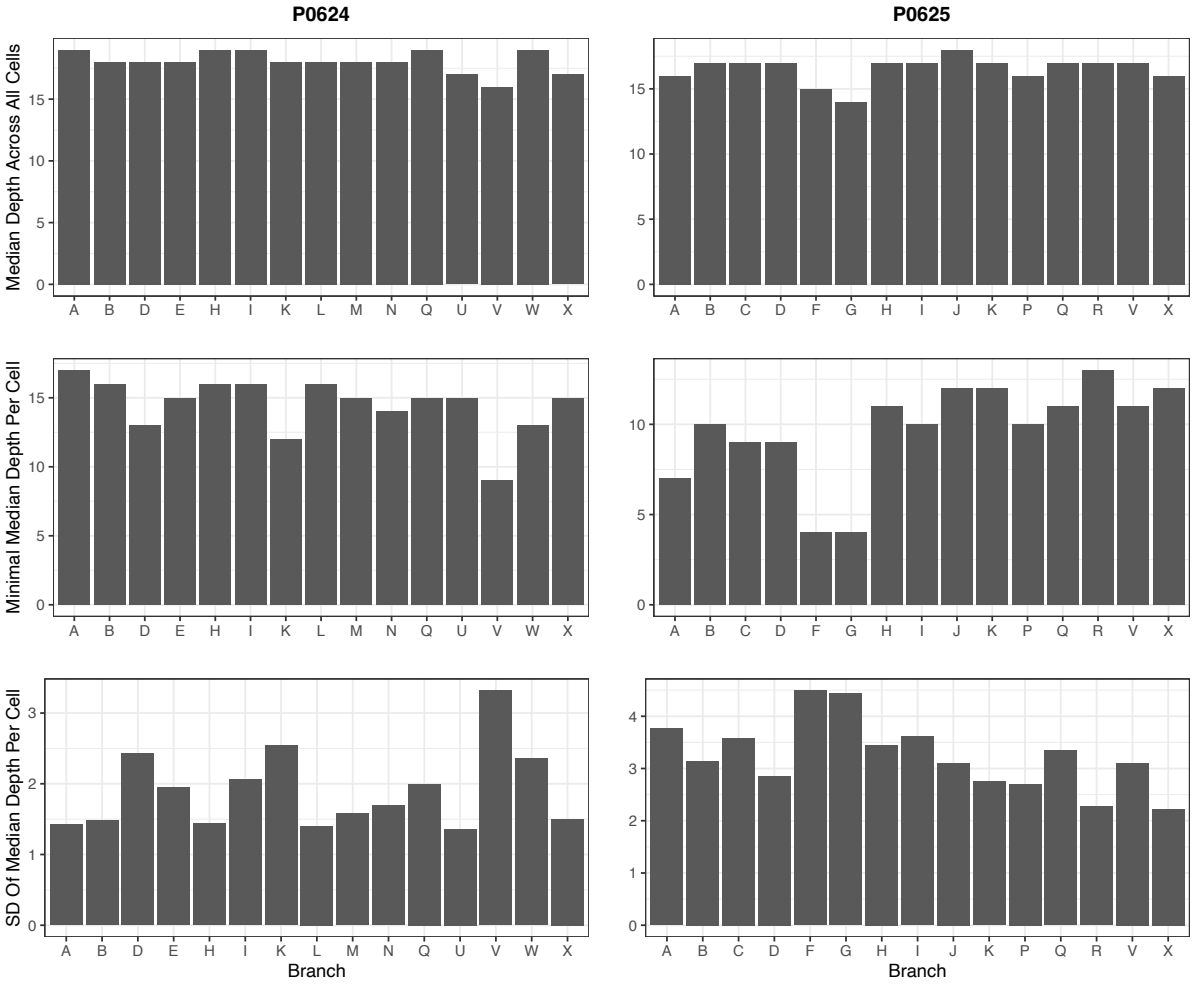

Supplementary figure S9. Branch-specific quality metrics for single-cell WGS data. Quality metrics for the branches of the lineage trees depicted in supplementary figure S10 (P0624, left column) and figure 6 (P0625, right column). The letter corresponding to each branch is displayed on the x-axis. The first row shows the median depth in each branch. The second row shows the minimal median depth in each branch. The third row shows the standard deviation of median depth in each branch.

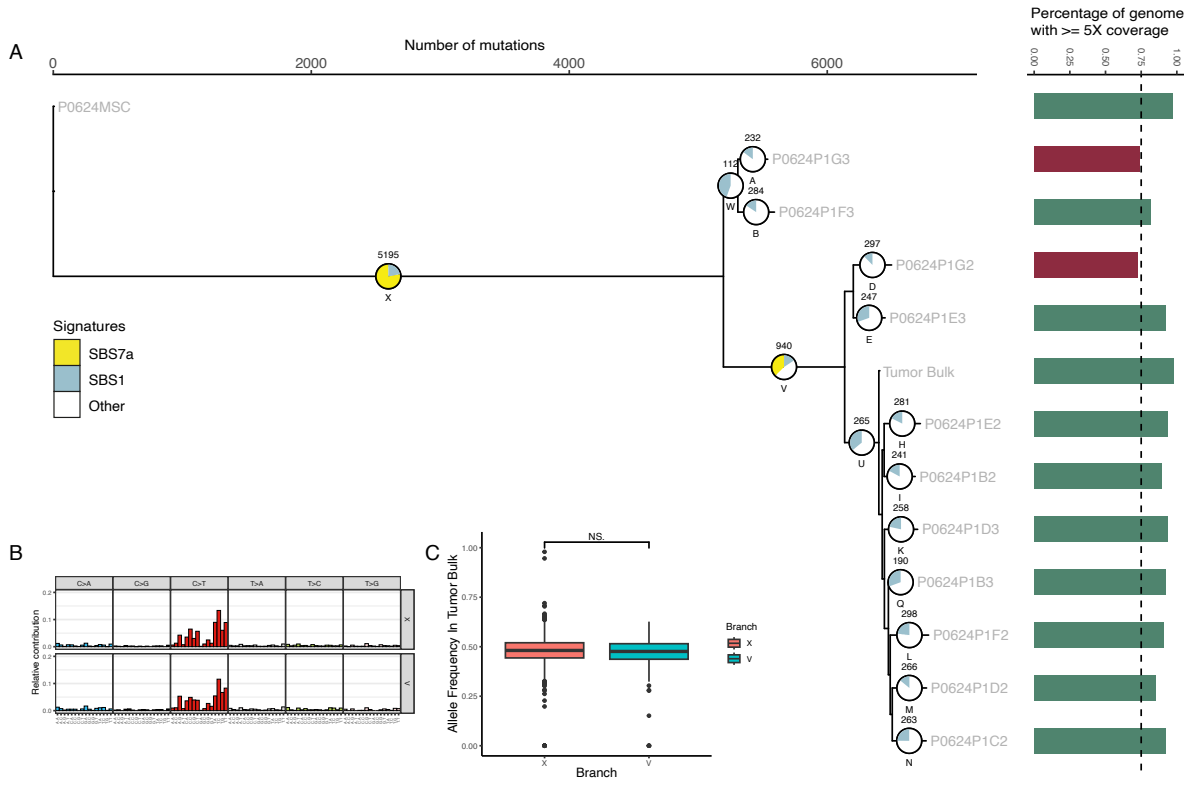

Supplementary figure S10. Lineage tree based on the single cell WGS data of patient P0624. A) Lineage tree. The trunk of the lineage tree shows the number of shared mutations between all following clones. If a clone branches off, it means that it shares no more mutations with other clones. The number of mutations is depicted above each branch along with a pie chart that shows the percentage of mutations associated with each mutational signature. SBS7a is shown in yellow, SBS1 is shown in blue and other mutational signatures are shown in white. To the right of the lineage tree is a bar plot corresponding to each clone in the lineage tree. This bar plot shows whether over 75% of the genome is covered with a depth of at least 5 (green bars). B) Mutational profiles of each group of shared mutations that had a contribution of SBS7a. C) Boxplot that shows the allele frequency for each group of shared mutations that contained SBS7a-associated mutations.